The Natural History and Genotypes of Choroideremia

by

Paul Richard Freund

A thesis submitted in partial fulfilment of the requirements for the degree of

Master of Science

Medical Sciences - Ophthalmology
University of Alberta

Abstract

Choroideremia (CHM) is an inherited X-linked retinal dystrophy that causes hemizygous males to develop nyctalopia and a progressive loss of their peripheral visual field until only central vision remains. At the end stages of the degeneration, central acuity is also affected. The onset and rate of the degeneration varies significantly among individuals. This study looked to establish a relationship between 66 pathogenic mutations in the *CHM* gene and their respective CHM phenotypes.

Cross-sectional analysis of the clinical data and genotypes of affected males did not show any genotype-phenotype correlations that could predict the observed variability. Analyses showed variable loss of visual acuity in individuals above 40 years of age, precluding its use as a sensitive marker of disease progression. Visual function was better monitored by width of visual field (by Goldmann perimetry or microperimetry), foveal sensitivity, or full-field stimulus threshold. This will be pertinent for monitoring and evaluating clinical trials of gene therapy.

Preface

This thesis is an original work by Paul Freund. The research project, of which this thesis is a part, received research ethics approval from the University of Alberta Research Ethics Board, “Choroideremia: expanding the phenotype and genotype”, No. Pro00005194. Part of the research conducted in this thesis was part of a collaboration with Dr. Yuri Sergeev at the National Eye Institute, USA. Dr. Sergeev assisted by conducting the *in silico* protein modelling of REP-1.

Acknowledgements

My work on my MSc could not have been completed without the significant advice, support, and encouragement from those around me. I am deeply indebted to Dr. Ian MacDonald for providing me with the invaluable opportunity to join him in his research on choroideremia and realize my aspirations to enter the field of ophthalmology. Dr. Yves Sauvé has been a wonderful mentor since meeting him 8 years ago, providing guidance not only for my education and career, but other important aspects of life such as cooking! I also must thank Dr. Matt Tennant and Dr. Stacey Hume for their excellent feedback as members of my committee.

Thank you to Dr. Yuri Sergeev for generously assisting me with his expertise in computer modelling of proteins. Jackie Mewes-Arès, Alina Radziwon, Stephanie Chan, and Mira Furgoch were excellent lab & office-mates who were always willing to discuss and help me through interesting topics that came up in the course of my research. I also sincerely appreciate the work of Dr. John Dimopoulous and Ishrat Gill for their work with establishing normal parameters and optimizing the lab equipment.

I'd also extend my thanks and appreciation to the choroideremia community and their research foundations. Their enthusiasm and support for my research has been essential, with many members of the community donating their valuable time to participate in the ongoing study and characterization of their disease.

My family has been a fount of support: my lovely fiancée, Kathleen O'Connor, has offered unconditional support and assistance, in addition to applying her counselling and therapy training. My parents generously accepted me back into their home and provided all of the necessities that made my life much easier, permitting me to complete this degree within its shortened timeline. I greatly appreciate all of their efforts and contributions.

Table of Contents

Tables

Figures

Acronyms and Abbreviations

ABCA4 – ABCA4 ATP-binding cassette, sub-family A (ABC1), member 4 gene (human)
AMD – Age-related macular degeneration
RBP – Rab binding platform
cDNA – Complementary deoxyribonucleic acid
CF – Counting fingers visual acuity
CHM – Choroideremia
CHM – Choroideremia (Rab escort protein 1) gene (human)
CHML – Choroideremia-like (Rab escort protein 2) gene (human)
DNA – Deoxyribonucleic acid
ERG – Electroretinogram
FAF – Fundus autofluorescence
FST – Full-field stimulus threshold
GDI – Guanine nucleotide dissociation inhibitor
GGTase-2 – Geranylgeranyltransferase 2
GGPP – Geranylgeranylpyrophosphate
GTP – Guanosine triphosphate
HGMD – Human Genome Mutation Database
HM – Hand-motion visual acuity
HSF – Human Splice Finder 3.0
INL – Inner nuclear layer
IS – Inner segments
kb – Kilobases
kDa – Kilodaltons
LCA-2 – Leber congential amaurosis – type 2
logMAR – Logarithm of the minimal angle of resolution
LP – Light perception visual acuity
MERTK – C-mer proto-oncogene tyrosine kinase gene (human)
NMD – Nonsense-mediated decay
NLP – No light perception visual acuity
OCT – Optical coherence tomography
ONL – Outer nuclear layer
OD – Oculus dexter (right eye)
OS – Oculus sinister (left eye)
OS – Outer segments
OU – Oculus uterque (both eyes)
RBP – Rab binding platform
REP-1 – Rab escort protein 1
REP-2 – Rab escort protein 2
RGC – Retinal ganglion cell
RNFL – Retinal nerve fibre layer
RPE – Retinal pigment epithelium

RPE65 – Retinal pigment epithelium-specific protein 65kDa
RPE65 – Retinal pigment epithelium-specific protein 65kDa gene (human)
SNP – Single nucleotide polymorphism
tRNA – Transfer ribonucleic acid
UPR – Unfolded protein response
VA – Visual acuity
VF – Visual field

Introduction

Choroideremia (CHM; infrequently called progressive tapetochoroidal degeneration or choroidal sclerosis) is an inherited retinal disorder first described by Mauthner in 1871[1]. CHM is characterized by the degeneration of photoreceptors, retinal pigment epithelium (RPE), and ultimately the choroid, resulting in nyctalopia, loss of peripheral vision, and blindness[2]. Its prevalence is estimated to be 1/50 000 − 1/100 000[2, 3]. CHM is an X-linked disorder that is 100% penetrant in hemizygous males; female carriers are typically asymptomatic, though they can also exhibit similar severe retinal degeneration[2]. CHM is only known to be caused by mutations in the *CHM* gene, which encodes for Rab escort protein 1 (REP-1). REP-1 is ubiquitously expressed in all tissues of the human body, but the only clinically significant phenotype is retinal degeneration.

Clinical Description

Hemizygous Males

The first symptom of CHM is nyctalopia, which is typically noticed by affected males by their teenage years [4]. Concurrently, a ring scotoma develops in the periphery of individuals' visual fields (VFs) and expands towards their central vision. This field constriction becomes symptomatic by 20 years of age and continues to progress relatively symmetrically in both eyes. Despite the loss of peripheral vision, patients are able to function very well due to stable visual acuity (VA): they maintain the ability to read and work with the caveat that assistance is needed for activities requiring

peripheral vision (*e.g.*, navigating unfamiliar buildings, scanning for specific visual targets, *etc.*). The rate of decrease in VA, calculated over the entire course of the disease, is 0.006 to 0.018 logMAR units/year [4, 5]. Beyond 50 years of age, VA declines at an increased rate of 0.02 logMAR units/year, suggesting that VA decreases more slowly in the early stages of CHM before declining faster in the late stages of the disease [5]. However, there is significant variation between affected individuals (even within families) and individuals in their 6th decade can have VA ranging from 20/20 to hand-motion (HM) [4-6].

A large study of affected Scandinavians (with clinical diagnoses of CHM) by Kärnä described changes in VF using an ordinal scale [7]. Generally, young males (<20 years old) had decreased sensitivity and enlarged blind spots and males older than 20 years of age started to develop annular scotomas. Males spanning 40 to 60 years of age had a wide range of VF scores, ranging from enlarged blind spots with diminished sensitivity to only central vision remaining. Quantifying dynamic Goldmann VF results in a Danish cohort showed deterioration above the age of 20 years, albeit with significant inter-individual variation, similar to the findings of Kärnä [8]. Hirakawa *et al.* showed a linear decrease in VF sensitivity over time in advanced CHM using automated 10-2 Humphrey VF testing, but did not comment on the size of the VF [9].

Kärnä also quantified the degree of nyctalopia using dark adaptometry and an ordinal grading system [7]. There was significant variation in the rate and extent of dark adaptation deterioration with respect to age: 10 year old males ranged from normal adaptation to monophasic cone adaptation only. The ordinal scale and variability

observed precludes further comment on the severity of the nyctalopia in adults beyond confirming its presence.

On examination, males have characteristic fundus changes: salt and pepper mottling of the RPE develops into loss of large areas of RPE and retina in the periphery, exposing the choroidal vasculature beneath (Fig. 1-1A). Eventually, the choroid also degenerates and only bare sclera is visible (Fig 1-1B). A macular island of intact retina and RPE remains until the late stages when the island also degenerates. Fundus autofluorescence (FAF) can be used to delineate the area of surviving RPE tissue since the RPE island will ultimately be the only remaining location of lipofuscin fluorophores [10, 11]. As a result, the RPE tissue will appear as an island of relative hyperfluorescence on a non-fluorescing background (Fig. 1-1C). Intravenous fluorescein angiography (IVFA) will show the opposite: hyperfluorescence through severe window defects in the periphery with relatively low signal from the intact RPE [12, 13]. Window defects may exist in areas of RPE that appear intact on visual exam, suggesting that these areas of RPE are dysfunctional and at higher risk of future degeneration. Due to the invasiveness and risks associated with IVFA, FAF is the preferred technique for serial monitoring of CHM progression.

Optical coherence tomography (OCT) shows the loss of the outer nuclear layer (ONL), the photoreceptor inner and outer segments (IS and OS), RPE, and thinning of the choroid that corresponds to visible fundus changes (Fig. 1-1D). The loss of photoreceptor OS precedes thinning of the ONL and RPE [14]. OCT scans in young males can show thickening of the retina prior to loss of the ONL, IS/OS, and the RPE layers [15].

This retinal thickening is postulated to be the result of early photoreceptor injury or inflammation causing activation of Müller cells. The inner layers of the retina (retinal nerve fibre layer (RNFL), retinal ganglion cell (RGC) layer, and inner nuclear layer (INL)) only undergo atrophy at the end stage of the disease, despite the early loss of the upstream photoreceptors [16].

Electoretinography (ERG) demonstrates a loss of rod activity (decreased b-wave amplitudes in response to dim flashes under dark-adapted conditions) preceding the loss of cone function [10, 17]. The rapid loss of an ERG signal (ERGs are frequently not recordable by 30 years of age) is due to the death of photoreceptors; the small central retinal island in middle or late stages of CHM cannot generate a large enough mass potential to be recorded by the surface electrodes in ERG testing. Thus, ERG can be used in the diagnosis of CHM in young males, but does not serve a significant role in the monitoring of advanced CHM.

Increased light scatter from posterior subcortical lens irregularities correlates with the extent of retinal degeneration in CHM. The light scatter is not a significant contributor to decreased visual acuity, but can aggravate the poor vision of affected males by increasing glare in specific situations (*e.g.*, while travelling in cars or in snowy conditions) [18, 19].

Heterozygous Females

The phenotype of heterozygous females is usually mild and does not include clinically significant VA or VF changes [5, 20]. Mottling of the peripheral fundus, more visible with FAF, may be the only sign that a female is a carrier [21]. These peripheral changes are

similar to the early changes observed in males but, while the mottling can become more prominent with age in carriers, most carriers do not develop photoreceptor or RPE degeneration [22]. Subclinical multifocal ERG changes can be detected in the cone system, but full-field ERGs are typically normal [21, 23]. This electrophysiological finding is consistent with microperimetry results (in an unrelated sample of carriers), which showed that carriers were found to have focal areas of decreased macular sensitivity relative to a control group [24]. However, should unbalanced lyonization cause a higher proportion of retinal cells to inactivate the chromosome containing the functional *CHM* gene, female carriers may develop the classic signs and symptoms of CHM [25-27]. The symptoms of affected carriers can range in severity from mild nyctalopia at advanced ages to a phenotype indistinguishable from males.

Pathophysiology

Histopathology

Despite its name, CHM is not a primary disorder of the choroid, but characterized by an initial degeneration of photoreceptors and RPE tissue [28, 29]. The mechanism by which *CHM* mutations cause retinal degeneration has not been determined, but several potential pathways have been identified and likely occur in concert. In CHM, altered phagocytosis by RPE cells prevents the proper interaction between rod OS and the RPE, causing an accumulation of OS material at the level of the RPE [30, 31]. The RPE functions to phagocytose rod OS, recycle *trans*-retinal to *cis*-retinal, regulate the retinal environment to ensure photoreceptor health and function, and form the blood-retina barrier

(necessary for maintaining the retina's immuno-priveledged status) [32]. However, a tissue-specific knock-out model of CHM demonstrated that RPE dysfunction is not the sole cause of choroideremia and that outer retinal degeneration occurs even when only photoreceptor REP-1 expression is knocked-out [33]. Degeneration accelerates in a synergistic fashion if REP-1 is absent in both photoreceptors and RPE cells.

The loss of REP-1 also results in increased systemic serum levels of inflammatory cytokines, which correlates with disease severity *in vitro* and *in vivo* [30, 34]. As previously mentioned, inflammatory stimulation of Müller cells is postulated to be the cause of the early retinal thickening observed in affected males [15]. Inflammatory cells have also been found in post-mortem tissue in an affected male and female carriers [35, 36]. Altered RPE activity and a pro-inflammatory microenvironment both contribute to the development of CHM. Photoreceptor tubulations are found in high-resolution OCT imaging and pathology specimens [35, 37]. Outer retina tubulations are believed to be part of the final common pathway of photoreceptor degeneration and are present in other degenerative retinal disorders such as retinitis pigmentosa, pattern dystrophy, and AMD [38].

Molecular Pathogenesis

REP-1 is an obligatory chaperone protein in the post-translation modification of Rab GTPases (ras genes from rat brain), a necessary process for proper trafficking and localization of the Rab proteins (Fig. 1-2). REP-1 is responsible for recognizing and orientating Rab proteins appropriately with respect to the catalytic pocket of Rab geranylgeranyltransferase 2 (GGTase-2) to facilitate Rab prenylation [39]. REP-1 initially forms a complex with GGTase-2, a heterodimer enzyme consisting of α and β subunits.

REP-1 then binds to Rab proteins via its Rab binding platform (RBP) and guides the flexible Rab C-terminus tail towards the active site of the Rab GGTase-2 [40]. Alternatively, the REP-1 protein can associate with the Rab protein prior to forming a complex with GGTase-2, though this pathway is not as energetically favourable and occurs less frequently [41]. When the Rab protein is properly aligned within the Rab:REP-1:GGTase-2 complex, the GGTase-2 sequentially binds one or two geranylgeranylpyrophosphate (GGPP) fatty acids to the Rab protein C-terminus. After dissociation of the Rab:GGPP:REP-1:GGTase-2 complex, the Rab-GG is escorted by REP-1 to its target membrane, with the REP-1 shielding the hydrophobic GG moieties from the cytoplasm. When Rab-GG:REP-1 dissociate, the GG fatty acids provide a hydrophobic membrane anchor for the otherwise hydrophilic Rab protein.

The Rab family consists of 60+ proteins, which facilitate endocytosis, exocytosis, intracellular trafficking of vesicles, and generation of organelles [42]. The underprenylation of Rab proteins has been implicated as the cause of retinal degeneration in CHM [6, 43]. Decreased prenylation, due to the absence of REP-1, causes reduced phagocytosis and proteolytic degradation in monocytes [31]. Similar phagocytic dysfunction in RPE cells explains the histopathologic changes discussed above. Supporting this theory, Rab27a is expressed in the RPE tissue and relatively underprenylated in CHM compared to other Rab proteins [44, 45]. However, Rab27a is not involved in the phagosome or lysosome pathways that are necessary for RPE phagocytosis. Furthermore, Griscelli syndrome Type II, a disorder of hypopigmentation and T-cell dysfunction, is caused by mutations in Rab27a and lacks an ocular phenotype [46, 47]. Thus, Rab27a underprenylation may

contribute to the sparse fundus pigment in CHM (in comparison to the pigment bone spicules that characterize retinitis pigmentosa), but Rab27a underprenylation is unlikely to be the sole cause of retinal degeneration in CHM. Other Rab proteins, such as Rab7, which contribute to impaired lysosome acidification are also affected in CHM [30].

Impaired lysosome acidification and decreased capacity for functional phagocytosis and degradation may contribute to the pro-inflammatory environment and cause the accelerated development of age-related macular degeneration (AMD) features in the CHM mouse model [35, 36, 48, 49]. Underprenylation and its putative effects on RPE dysfunction and inflammation require further investigation to delineate the exact pathways that cause the development of CHM.

Rab Escort Proteins

REP-1 belongs to a family of proteins that share a common Rab binding platform (RBP) that enables REP-1 to associate with Rab proteins. A closely related paralogue, Rab Escort Protein 2 (REP-2), is encoded by the *CHM-like* (*CHML*) gene. REP-1 and REP-2 have similar roles in prenylation of Rab proteins, but have different binding affinities and tissue specific regulation of their activity [50, 51]. The prenylation activity of REP-2 is almost sufficient to compensate for the absence of REP-1 in CHM, with the only clinically significant phenotype being retinal degeneration. However, subclinical biochemical phenotypes do exist in other tissues: *in vitro* fibroblast and lymphoblast cells cultured from affected males have detectable differences in the rate of Rab prenylation [31, 43]. The retina is likely a watershed area where compensatory REP-2 activity is insufficient due to

differential Rab expression and regulation of prenylation, resulting in ocular phenotype of CHM.

A third protein, guanine nucleotide dissociation inhibitor (GDI), shares the RBP motif with REP-1 and REP-2 [52]. Its primary function is to associate with prenylated Rab GTPases and shuttle inactive Rab proteins back to the cytosol where the Rab proteins enter the prenylation cycle again [53]. GDI has a higher affinity for prenylated Rab proteins compared to REP-1 or REP-2 but cannot form complexes with GGTase-2, so GDI proteins cannot compensate for reduced prenylation in CHM [54].

The REP-1 protein structure has been solved using x-ray crystallography of rat rep-1 in complex with rab-GGTase-2 and rab7 molecules [55, 56]. A 2-domain model of REP-1 was proposed, with domain 1 forming the RBP with multiple α-helices and β-sheets and domain 2 interacting with GGTase-2 (Fig. 1-3). An alternative 3-domain structural model of human REP-1 was later proposed by Sergeev *et al.*, which separates the globular domain 1 into two distinct domains [57]. Both of these domains make up the RBP and have interactions with Rab proteins.

CHM/REP-1 Mutations

The *CHM* gene consists of 15 exons located at the Xq21.1 position [58-60]. *CHM* spans 186 kb, but encodes an mRNA transcript that is only 5.6 kb long. The resultant REP-1 protein is 653 amino acids long. In the most extensive *CHM* mutation database, 133 unique variants (including 2 non-pathogenic variants) have been documented (Retinal and hearing impairment genetic mutation database, available at: http://www.lovd.nl/CHM). The frequency of *CHM* mutations is highly skewed towards nonsense mutations,

deletions or insertions causing frameshifts, and splice site mutations that result in the premature truncation of REP-1. In these cases of prematurely truncated mRNA, mutant *CHM* mRNA undergoes nonsense-mediated decay (NMD) or translated, prematurely truncated REP-1 protein activates the cellular unfolded protein response (UPR) causing protein degradation [61-63]. As a result, there is a nearly universal absence of REP-1 protein in CHM.

In the five reported cases of missense mutations, two mutations (c.1520A>G (p.His507Arg) and c.1649T>C (p.Leu550Pro)) have very low levels of REP-1 expression compared to normal controls on immunoblot analysis [6, 57]. The REP-1$^{p.His507Arg}$ did not bind with GGTase-2 and is considered non-functional; REP-1$^{p.Leu550Pro}$ expression was only detected at very low levels in fibroblast cultures and was undetectable in lymphoblasts. A c.1412A>T mutation was initially predicted to result in a p.Gln471Leu substitution, but further analysis revealed it affects the 3' splice site of exon 11, causing skipping of exon 11 and a prematurely truncated transcript without REP-1 expression [64, 65]. A reported c.940G>A (p.Gly314Arg) mutation alters the 3' splice site of exon 7, but has not undergone any further workup to examine the transcribed mRNA sequence, REP-1 expression, or REP-1 activity (NGRL, Manchester LOVD, available at: https://secure.ngrl.org.uk/LOVDv.2.0/home.php). A c.104T>C (p.Leu35Pro) missense mutation is reported in the Manchester database and also lacks functional or expression analysis. However, given the drastic substitution of a very hydrophilic and inflexible proline residue in place of a very hydrophobic leucine residue, the mutation likely has a significant effect on protein structure and may also result in misfolded or non-functional

REP-1. In summary, despite a small number of REP-1 mutations with missense mutations, there are no confirmed cases of CHM with normal REP-1 expression or a partially functioning REP-1 protein.

Due to the length of the *CHM* introns, genetic testing of *CHM* is typically limited to sequencing only the exons and their immediate flanking regions [66]. Direct sequencing of the exons has 78% detection rate in males with a clinical diagnosis of CHM and 50% detection in symptomatic females or obligate carriers [66]. If sequencing fails to detect *CHM* mutations, alternative techniques can be employed, including multiplex ligation-dependent probe amplification (MLPA) to detect copy number variations (*e.g.*, exon duplications or deletions in carriers, or exon duplications in males) and immunoblot assays for the presence of REP-1 [67-69]. Immunoblot assays for the presence of REP-1 are very specific and sensitive (100% in a study of 16 males) in males because of the rarity of REP-1 expressing *CHM* mutations [6, 57, 69, 70]. Heterozygous females will express REP-1 in sufficient quantities that immunoblot assays are not diagnostically useful; however, MLPA can be used in cases where direct sequencing is negative for a mutation.

The *CHML* gene for REP-2 is 2.0 kb in length, located on chromosome 1 at 1q42 [71]. Despite the 75% homology (96% homology if excluding conservative amino acid substitutions) and overlap in function between REP-2 and REP-1, there are no known mutations in *CHML* that result in disease.

CHM Therapies & Clinical Trials

Translational Bypass Therapy

Aminoglycosides (*e.g.*, gentamicin or paromomycin) are bacteriocidal antibiotics that alter the fidelity of mRNA translation. By changing the fidelity of bacterial 30S ribosome subunits, aminoglycosides cause incorrect protein translation that results in bacterial cell death [72]. However, aminoglycosides also bind to the 40S subunit of eukaryotic ribosomes and reduce the fidelity of the translation process, causing a failure to recognize stop codons. This process, translational bypass of stop codons, occurs via insertion of a near-cognate tRNA instead of halting translation with class I release factors. As a result, prematurely truncated proteins can be translated to a full-length protein. This can restore protein function in diseases caused by nonsense mutations such as cystic fibrosis and Duchenne muscular dystrophy [73, 74]. However, high-dose or prolonged aminoglycoside therapy is associated with severe side effects such as ototoxicity and nephrotoxicity, as well as the inconvenience of requiring parenteral administration. PTC-124 (Ataluren), an aminoglycoside derivative, is an oral agent that is neither oto- nor nephrotoxic and has increased read-through potential compared to traditional aminoglycosides [75]. Phase I/II clinical trials were successful in treating cystic fibrosis and a Phase III trial was recently completed (ClinicalTrials.gov #NCT00803205) [76]. A trial treating Duchenne and Becker muscular dystrophies was stopped early due to lack of efficacy (ClinicalTrials.gov #NCT01009294). Translational bypass therapy may have a role in the treatment of CHM as nonsense mutations make up 35% (92/262

mutations) of mutations reported in the CHM/REP-1 LOVD database (http://www.lovd.nl/CHM).

In a zebrafish model of CHM, *chm*$^{-/-}$ fish embryos are not viable beyond 5 days post fertilisation as they lack a copy of an equivalent *chml* gene encoding rep-2 [77, 78]. However, a single dose of gentamicin can extend the survival of *chm*$^{-/-}$ zebrafish to 9 days post fertilisation [79]. In addition to prolonged survival, treated zebrafish also develop normal retinal lamination, an intact RPE, and thicker INL and RGC layers compared to untreated zebrafish. Translational bypass therapy has also been applied to other animal models of retinal degenerations. Gentamicin treatment increased photoreceptor numbers and ERG responses in a *Rho*$^{p.Ser334*}$ mouse model of retinitis pigmentosa (but failed to have similar positive effects in an alternate *Rd12* mouse model). Ataluren-treated mice are able to bypass a premature stop codon (p.Arg31*) and synthesize full-length protein *in vivo* in the *ush1c* mouse model of Usher Syndrome [80, 81].

Translational bypass therapy has potential to treat CHM, but requires additional investigations to assess its effects in the murine CHM model and hemizygous human CHM fibroblast or lymphoblast cultures. Further, translational bypass therapy is not a universal treatment for CHM because only a third of affected males would be eligible. The frequency of successful translational bypass also depends on the premature stop codon and its adjacent nucleotides, which would further limit the pool of individuals who could be successfully treated [82].

Gene Therapy

Gene therapy, the insertion of functional copies of genes into cells, is a rapidly advancing area of medicine. It holds the promise of being able to permanently reverse genetic defects in individuals to improve or cure the signs and symptoms of inherited diseases. The transfer of exogenous genetic material into targeted cells relies on the use of vectors as vehicles to deliver the payload into cells. A variety of vectors, capable of carrying DNA payloads and transfecting targeted cells, have been identified and used in gene therapy, such as adenovirus, adeno-associated virus (AAV), lentivirus, nanoparticles and polymer vehicles. Each vector has different immunogenicity, cell specificity, transfection rates, expression stability, and payload capacity. These factors must be taken in consideration given that different tissues and diseases may have different vector requirements. For example, in choroideremia, successful gene therapy requires a vector that can target, transfect, and express protein in non-dividing cell types (*i.e.,* photoreceptors and RPE), as well as maintain stable long-term protein expression. AAV vectors can transfect different cells in the retina depending on their serotype (*e.g.*, AAV2/5 transduces both photoreceptors and RPE, whereas AAV2/1 only transduces RPE cells) and lack the immunogenicity that characterizes adenoviruses [83]. Further, cell-specific transfection allows for the use of strong universal promoters (compared to weak cell specific or gene specific promotors that are necessary in non-specific vectors) to ensure sufficient protein expression. One notable limitation of the AAV vector is its restricted payload capacity – the maximum length of the gene and its

promoters is 4.7 kb) [84]. The *CHM* cDNA is 2.5 kb long, small enough that the gene and its promoters can fit within the 4.7 kb payload capacity of the AAV vector [85].

The eye has been identified as a target organ for gene therapy as it has several inherent properties that overcome some of the problems related to systemic gene therapy, such as the immunogenicity of the vectors used in gene therapy, which can cause serious side effects including death [86, 87]. The eye is an immunoprivileged organ with the blood-ocular barrier, which minimizes exposure of exogenous vectors to systemic circulation and prevents sensitization or stimulation of the systemic immune system. The blood-ocular barrier also prevents the widespread dissemination of locally administered vectors throughout the body, so that lower dosages can be used while still maintaining efficient transfection rates. Another positive feature of the eye is that the administration of the drug can be directly visualized and follow-up can be done with non-invasive ophthalmological testing.

The treatment of Leber congenital amaurosis - type 2 (LCA-2) with ocular gene therapy was a key proof-of-principle for ocular gene therapy with regards to both the safety and efficacy in treating inherited retinal dystrophies [88-90]. LCA-2 is caused by mutations in the retinal pigment epithelium-specific protein 65 kDa gene (*RPE65*) and causes rapid retinal degeneration resulting in blindness, often before 6 months of age [91]. With treatment of individuals affected by LCA-2 with a subretinal injection of AAV2 carrying *RPE65* cDNA, dramatic functional improvements and partial restoration of vision have been observed. The functional and anatomical improvements observed in treated eyes are very promising, but questions remain regarding the stability of the

gene therapy and whether it is able to permanently halt disease progression [92]. Nevertheless, with the early successes of the LCA-2 clinical trials, Phase I and II clinical trials have been undertaken examining gene therapy in gyrate atrophy (ClinicalTrials.gov #NCT00001735), AMD (#NCT01024998, #NCT01301443), Stargardt macular degeneration (#NCT01367444), Usher syndrome Type 1B (#NCT01505062), *MERTK*-associated retinitis pigmentosa (#NCT01482195), and CHM (#NCT01461213).

CHM is an ideal target for gene therapy due to its primary degeneration being limited to the photoreceptors and RPE cell layers of the retina, as well as the extended time course of its degeneration. The photoreceptors and RPE tissues are targeted by the same AAV2 vector used in the LCA-2 trials, which has a very good safety profile and is able to transfect both cell types [93]. The protracted natural history of CHM suggests that there is a very large window of opportunity where there will still be functional macular photoreceptor and RPE tissue to be rescued, which is corroborated by OCT imaging [14, 15]. There has been little study of retinal remodelling in CHM, but the inner retinal layers (RGC and RNFL) and cortical visual areas are preserved and retain functional activity (demonstrated by the Argus II epiretinal prosthesis) [94]. Thus, gene therapy can potentially rescue the surviving, viable photoreceptors and RPE that make up the outer retina, with confidence that the inner retina is still functional. Treated patients with choroideremia should be able to maintain very good VA due to these factors (compared to LCA-2 where degeneration is rapid and gene therapy can only partially reverse VA loss) [95]. However, outside of the surviving retinal island, there is no capacity to

regenerate photoreceptors and reverse the peripheral degeneration using gene therapy.

Preclinical studies of CHM in a conditional knock-out mouse model showed a restoration of prenylation activity with a REP-1-lentivirus vector and improved ERG function with a REP-1-AAV2/2 vector [96, 97]. Human CHM fibroblasts, lymphoblasts, and retinal explants have also been successfully treated with REP-1-AAV2 *in vitro* and have high levels of prenylation activity [85, 98]. Early results from 6 individuals in the Phase I/II CHM clinical trial for CHM gene therapy showed that the subretinal injection of fluid with REP-1-AAV2/2 can be safely performed and VA returned at least to baseline within 1 month [99].

Study Goals

This study has two main goals:

1. Assess whether genotype-phenotype correlations can account for the clinical variability observed in choroideremia.
2. Define the natural history of choroideremia in a large sample and assess two new outcome measures (full-field stimulus threshold and microperimetry) in anticipation of upcoming clinical trials for treating choroideremia.

The onset of symptoms, rate of progression, and severity of disability varies dramatically in affected males in choroideremia. The large number of *CHM* mutations (>130 different reported mutations) may account for the phenotypic variability observed, in a similar manner to the *ABCA4* gene variants and Stargardt disease [100]. However, given that the majority of mutations are null mutations and lack any detectable expression of REP-1,

the REP-1 activity should be uniformly non-existent and no genotype-phenotype correlation will exist. Confirmation of the lack of a genotype-phenotype correlation that has been previously postulated on the basis of small case studies and clinical experience would assist the selection of participants for clinical trials. Other features of potential participants (such as age and current visual function) may be more pertinent to their selection and treatment than their specific *CHM* mutation.

Prior to the development of gene therapy trials, there was no effective treatment offered for individuals with inherited retinal disorders such as CHM. Treatment is generally limited to monitoring for secondary complications (*e.g.*, cystoid macular edema or macular holes) and facilitating access to low-vision resources [101-103]. As a result, there was no impetus to define or track the longitudinal visual changes beyond small case reports, nor were there technical solutions to accurately assess severely blind individuals such as those in the late stages of CHM. However, in order to follow individuals treated with gene therapy (or potentially translational bypass therapy in the future) and assess changes in vision post-treatment, accurate metrics must be developed that are specific to choroideremia [104, 105]. Concurrent with the development of gene therapy trials in retinal degenerations, there have been advances in assessment tools for use in severely blind individuals, such as full-field stimulus threshold (FST) testing and microperimetry [106-108]. By combining a retrospective review of affected males assessed via traditional measures (VA and Goldmann VF) with an analysis of additional novel testing modalities (FST and microperimetry), the natural history of CHM can be described in a more exact and quantitative fashion. This will facilitate the

monitoring of individuals treated with gene therapy and determine whether the clinical changes (or lack thereof) observed are normal for the slow degenerative process in CHM.

Materials & Methods

This study received ethics approval from the University of Alberta Health Research Ethics Board – Biomedical Panel. All procedures conformed to the Code of Ethics of the World Medical Association (Declaration of Helsinki).

Subjects

A review of the research files at the University of Alberta, Department of Ophthalmology and Visual Sciences collected 149 individual visit records for males and females with a confirmed mutation in the *CHM* gene and associated clinical data. A further 94 records with a molecular diagnosis of choroideremia were collected from the National Ophthalmic Disease Genotyping Network - eyeGENE® (National Eye Institute, Bethesda, MD). The combined 243 visit records and associated data were reviewed and 17 duplicate entries or visits without clinical data associated were excluded from analysis and the remaining 226 records were included.

Genotype Analysis

In order to analyze mutation frequency, only a single record from each family was included in the analysis. Records from follow-up visits from the same individuals were removed and in families with multiple individual records, only a single record was used. Families with benign *CHM* variants (silent mutations and polymorphisms detected in unaffected males) or that did not have a *CHM* mutation were also excluded. There were 106 family records included in this study.

Phenotype Analysis

A cross-sectional population of affected males was used to characterize the phenotype of choroideremia. Males with benign *CHM* variants and females were excluded. For males with multiple visits, the most recent visit was used. In cases where a test (*e.g.*, VF testing) was not done at the most recent visit, the most recent visit with that specific test was also included (any repeated tests were removed from this earlier visit's record). The cross-sectional analysis consisted of 132 individual visits (128 visits with VA and 64 visits with VF).

Longitudinal analyses were also performed on the subset of males with repeated visits. Males with benign *CHM* variants and females were excluded. 12 individuals were included and the number of visits ranged from 2 to 15 spanning 6 to 42 years.

Data

Genotype

Each record with a confirmed *CHM* mutation was reviewed and converted to standard coding DNA notation according to the Human Genome Variation Society guidelines [115]. Mutations were classified according to the Human Genome Mutation Database classifications (missense, nonsense, splice site, regulatory, small (≤20 bp) deletion, small (≤20 bp) insertion, small (≤20 bp) insertion/deletion (InDel), gross (>20 bp) deletion, gross (>20 bp) insertion, or other (including complex rearrangements and repeat variations)) [116].

The mutations were described by their location on the *CHM* gene using the exon or intron containing the mutation and mutated cDNA nucleotide. Mutations spanning multiple exons were identified by the earliest affected exon (*e.g.*, a deletion spanning exons 5-8 would be classified as occurring in exon 5). Likewise, mutations spanning multiple nucleotides were identified by the earliest affected nucleotide (*e.g.*, the same deletion of exons 5-8 would be classified as occurring at c.315T). Intronic mutations were identified by the next exonic nucleotide in the 3' downstream direction (*e.g.*, mutations affecting the donor and acceptor splice sites located on intron 4 would be classified as occurring at c.315T). The rationale for describing these mutations in this manner is that the *CHM* transcript will be abnormal downstream of the initial mutation location and likely prematurely truncated given the paucity of missense mutations in *CHM*. Thus, this will approximate the length of the truncated REP-1 protein. Consideration was also given to special cases (*e.g.*, whole gene deletions, missense mutations, and mutation clusters) in order to identify any irregular genotype-phenotype relationships that may have been overlooked through this statistical analysis.

REP-1 Modelling

The amino acid sequences of Rab proteins, geranylgeranyltransferase component A1, and REP-1 (RAE1_HUMAN) were retrieved from the UniProtKB database (http://www.uniprot.org/uniprot/P35556). The crystal structure of the rat REP-1 protein in a complex with C-terminally truncated Rab7 protein (PDB file: 1vg9) was used as a structural template for the structure of human REP-1 (residues 3 to 619, sequence

identity 73.4%). The human REP-1 was built by an automated protein-homology modelling Swiss-Model server with the QMEAN Z-Score: -1.253 [109].

The structure of the protein complex, which includes human REP-1, Rab7, and Rab GGTase-2, was generated using the corresponding rat structures as structural templates, (PDBfiles: 1vg0, 1ltx) as described by Sergeev *et al.* [57]. Mutant variant structures, p.Met443Val and p.Leu457Pro, were generated, refined and the effect of these mutations was simulated using a molecular visualization, modelling, and dynamics program YASARA [110, 111].

The impact of each missense mutation was analyzed with the Polyphen-2 program (http://genetics.bwh.harvard.edu/pph2) [112]. The PolyPhen-2 model was based on UniProtKB structure, RAE1_HUMAN, and the HumVar model was selected to maximize the relevance of the output to human disease. The SNAP model (http://www.rostlab.org/services/SNAP) was also used to predict any deleterious effects of missense mutations [113]. The SNAP model was based off the published primary structure of REP-1 [60]. Effects of missense mutations on splicing of the *CHM* transcript were evaluated using the Human Splice Finder 3.0 (HSF; http://www.umd.be/HSF3) [114]. Splice sites, branch points, enhancers, and silencers were all included in the HSF analyses.

Clinical Data

The clinical data was analyzed using the age (in years) of the individual at the time of assessment. The following variables were analyzed: the age (in years) when nyctalopia

was first noticed, the age (in years) when other visual symptoms (not including nyctalopia) were first noticed, the VA in the better eye, and the VF in the better eye. Missing variables were excluded pairwise from the analysis.

Snellen and decimal VA were converted to logMAR equivalents according to the following formula:

$$\text{logMAR equivalent} = -\log_{10}(\text{Decimal Acuity})$$

The decimal acuity is the Snellen fraction in decimal form (*e.g.*, 20/80 = 0.25). Semiquantiative VA were converted to logMAR equivalents as follows: counting fingers (CF) = 1.9, hand motion (HM) = 2.3, light perception (LP) = 2.7, no light perception (NLP) = 3.0 [117]. To best describe the residual visual function, the eye with better VA was included for analysis.

VF were quantified by the width of the continuous visual field across the horizontal meridian (in degrees) using a Goldmann perimeter with the III4e isopter. The physiological blind spot was not considered a break in the VF if the central field was continuous with the more peripheral field. VFs that were not performed with the III4e isopter were excluded. In the absence of Goldmann perimetry results, the central VF quantified with the Humphrey Field Analyzer (stimulus size III) or Centervue MAIA microperimeter was used. The eye with the better VF was included in the analysis.

Additional Testing Protocols

Full-field Stimulus Threshold Testing

The full-field stimulus threshold test (FST) was performed using the Diagnosys Espion system with a ColorDome full-field stimulator and the Diagnosys FST software (Diagnosys LLC, Lowell, MA). The parameters used have been previously described for use in low vision populations with retinal degenerations [106]. Briefly, participants' pupils were maximally dilated with 1% tropicamide and 2.5% phenylephrine ophthalmic drops and dark-adapted for 30 minutes prior to testing. Participants' non-tested eye was patched and both eyes were tested independently. The testing consisted of forced responses to stimuli (indicated by a tone) that was presented at varying intensities until the software could calculate a threshold with a Weibull function. The 0 decibel (dB) reference intensity was defined as 0.1 cd•s/m^2. Stimulus intensities ranged from -75 dB to +15 dB.

Each eye was tested three times with a white (65 000 K) stimulus, once with a blue (465 nm) stimulus, and once with a red (635 nm) stimulus. After the first threshold was determined, subsequent tests' starting intensities were adjusted to minimize the test duration. The results of the 3 white stimulus tests were averaged and the difference between the blue and red thresholds was calculated. Results were compared to normal reference ranges derived from individuals without any history of ophthalmic disease.

Microperimetry

Microperimetry was performed on the MAIA microperimeter according to the manufacturer's recommendations (Centervue, Padova, Italy). Patients were instructed and given a training test to ensure they were confident in the use of the microperimeter. Testing was performed in a dim room with undilated pupils and the non-tested eye was patched. The small fixation target was used unless the participants exhibited difficulty in finding and fixating on the target, in which case the large target or both targets were used as necessary. The expert 4-2 testing strategy was used with a non-standard 20° (41 stimulus) grid or a custom 11×11/20° (121 stimulus). The grids were centered over the visible retinal island in the macula. The results of the microperimetry were qualitatively assessed.

Analysis & Statistics

For statistical analyses, the threshold of $p<0.05$ was used to reject the null hypotheses. Post-hoc tests were corrected with the Bonferroni method to account for multiple comparisons.

Genotype Mutation Analysis

The frequency histograms for the *CHM* mutation analysis were created with GraphPad Prism (GraphPad Software Inc., La Jolla, CA). A Chi-square test statistic was applied to test for independence (IBM SPSS Statistics, Version 21, IBM Corp., Armonk, NY).

Cross-Sectional Analysis

The cross-sectional data was analyzed with GraphPad Prism with a modified form of the "inclusion/exclusion t-tests" technique described by Coussa *et al.* [5]. This technique determines the age at which VA begins to significantly deteriorate or the age after which the VF decreases at a linear rate. The sample population was divided at these two critical ages for the analyses of the VA and VF data.

Individuals were grouped by decade (1-10, 11-20,…, 71-80 years old) and Kruskal–Wallis one-way analyses of variance (ANOVAs) were performed. Dunn's multiple comparisons were performed to detect differences between the groups. If the two youngest age groups did not differ significantly ($p>0.05$), they were pooled and then the ANOVA/pooling technique was repeated in a stepwise manner. This continued until the pooled group was significantly different from the next oldest group. To ensure that the critical age was appropriate, linear regressions were performed at each iteration and the goodness of fit was assessed with the R^2 value for the subgroups. The critical age and resultant subgroups with the highest R^2 values were selected.

The subgroups (defined by the critical ages) were analyzed with multivariable linear regressions (IBM SPSS Statistics for Windows, Version 20.0, IBM Corp., Armonk, NY) with VA and VF as the dependent variables. A hierarchical regression model was used to enter predictors into the models and the forced entry method was used for each step. The predictors used were:

Step 1: Age

Step 2: First nucleotide affected by the mutation

Step 3: Age of onset of nyctalopia & Age of onset of other subjective symptoms

Longitudinal Analysis

Linear regressions were applied to model the 12 subjects with repeated visits with VA data and the 5 subjects with repeated VF data. The progressions of their VA and VF were compared to the predicted changes from the cross-sectional analyses.

Results

CHM Mutations Analyses

The genotypes of 106 unique families consisted of 66 different *CHM* mutations (Table 3-1). In comparison to all of the mutations recorded in the Human Genome Mutation Database (HGMD) for the entire human genome, *CHM* mutations have a significantly different distribution (Fig. 3-1; χ^2=133.4, df=9, p<0.0001)[116]. Nonsense mutations are more prevalent in CHM compared to the HGMD (*CHM* mutation frequency: 42%, HGMD: 11%). Conversely, missense mutations are far less likely to occur in CHM (CHM: 4%, HGMD: 45%). In this study, 3 families had a missense mutation (c.819G>T (p.Gln273His); c.1370T>C (p.Leu457Pro); c.1649T>C (p.Leu550Pro)) and one family had two missense mutations (c.238C>T (p.Leu80Phe) & c.1327A>G (p.Met443Val)). The c.1649T>C (p.Leu550Pro) mutation was previously reported [57]. The c.238C>T (p.Leu80Phe) substitution has been described as a variant of unknown significance with a minor allele frequency of 0.010 in the 1000Genome population (dbSNP #rs55741408).

The majority (73.5%) of the mutations detected result in prematurely truncated REP-1 protein due to nonsense or frameshift mutations. Splice site mutations and a regulatory mutation (p.Met1Ile) represent 14.1% of mutations. The precise effect of the splice site mutations on REP-1 translation cannot be predicted due to multiple potential outcomes (*e.g.*, exon skipping, novel splice site generation, *etc.*). Whole gene deletions are present in 8.5% of families (9 of the 21 gross deletions). The remaining 4% of mutations are the aforementioned missense mutations.

To assess for mutation hotspots in the *CHM* gene, the intron/exon locations were examined (Fig. 3-2). A disproportionate number of mutations (26/106 mutations) occur in exon 6. To account for the different lengths of exons, mutations were plotted with respect to the cDNA location at which they occur (Fig. 3-3). A cluster of 21 mutations occurs in the region spanning c.701-800 and 12 mutations occur in the region spanning c.801-900. This corresponds with exon 6, which spans c.703-819. Several of these mutations in exon 6 reoccur in multiple independent families: 2 families with c.715C>T (p.Arg239*), 10 families with c.757C>T (p.Arg253*), 5 families with c.799C>T (p.Arg267*), and 3 families with c.808C>T (p.Arg270*). The mutations c.817C>T (p.Gln273*) and c.819G>T (p.Gln273His) were found in one family each.

REP-1 Mutation Modelling

The three novel missense mutations were modelled *in silico* to predict their effects on REP-1 structure and function (Fig. 3-4). The p.Leu80Phe and p.Met443Val mutations in the REP-1 double mutant are located on the subdomain responsible for interacting with Rab7 (Fig. 3-5). The phenylalanine and valine residues introduced are similar in their hydrophobic properties to leucine and methionine, respectively, and these conservative substitutions are not likely to induce significant changes to REP-1 structure. Polyphen-2 HumVar predicted that the p.Leu80Phe substitution was benign (score 0.442, sensitivity 0.84, specificity 0.80) and SNAP predicted the substitution was neutral (Expected accuracy 60%). HSF predicted potential alteration of splicing via the creation of an exonic splicing silencer and alteration of exonic splicing enhancer regions. The p.Met443Val substitution was predicted to be neutral by both PolyPhen-2 and SNAP

(PolyPhen-2 score 0, sensitivity 1, specificity 0 and SNAP expected accuracy 53%). HSF predicted potential splicing changes due to generation of a potential donor site, as well as creation of new exonic silencer and enhancer sequences.

The p.Gln273His mutation is located in the GGPP binding pocket and will alter the dynamics of GGPP association with the REP-1:Rab7:GGTase2 complex. Polyphen-2 HumVar predicted this is a probably damaging mutation (score 0.951; sensitivity 0.64, specificity 0.92), however SNAP predicted this is a neutral substitution (Expected accuracy 53%). HSF predicted this mutation would most probably affect splicing by altering the existing donor site in exon 6.

The p.Leu457Phe mutation is located within a β-sheet; the inflexible proline residue will disturb the stability of the β-sheet, potentially destabilizing the entire REP-1 protein. PolyPhen-2 HumVar predicted this substitution to be probably damaging (score 0.99, sensitivity 0.09, specificity 0.99) and SNAP predicted this would be a non-neutral substitution (Expected accuracy 63%). There were no predicted splicing changes caused by this mutation.

Cross-sectional Analyses

Subjective Symptoms

Subjective symptoms of nyctalopia were self-reported in males at an average age of 12.6±1.0 years old (mean±SEM; Fig. 3-6). The average onset of other visual symptoms (including constriction of peripheral vision) was 19.7±1.3 years of age. Individuals with missense mutations or who are predicted to lack any *CHM* transcript or REP-1 protein

fragments (due to whole gene deletions or deletions spanning the ATG start codon on exon 1) were equally distributed around the mean, with no visible skew in their distribution. When compared to the location of the causative mutation on the *CHM* cDNA, there was no pattern between mutations and onset of symptoms (Fig. 3-7). Linear regression analyses confirmed the lack of association between genotype and phenotype (onset of nyctalopia p=0.29, onset of other visual symptoms p=0.47).

Visual Acuity

The VA from the better eye of 128 different affected males were grouped by age (when their vision was assessed) and the modified "inclusion/exclusion" test was applied to determine that the critical age for VA was 40 years old (Table 3-2; Fig. 3-8). VA was stable in males below 40 years of age (mean acuity ranges from 0.02 to 0.10 logMAR units), but VA declined above the critical age (Table 3-3).

Linear regression models (Fig. 3-9) predicted the rate of change in the VA of males ≤40 years old was not significantly different from 0 (p=0.71) and the change in the VA of males >40 years old was +0.0483 logMAR units/year (p=0.001). The rate of change in VA above 40 years of age corresponded to losing approximately 5 lines of acuity/decade on the Snellen chart. The cross-sectional data was heteroskedastic and the decline in VA above 40 years of age varied dramatically between individuals. Individuals who were predicted to lack any *CHM* transcript or REP-1 protein fragments (due to whole gene deletions or deletions spanning the ATG start codon on exon 1) showed the same variability as the other *CHM* mutations. Individuals harbouring

missense mutations in *CHM* demonstrated similar loss of VA to individuals with prematurely truncating mutations.

Multivariable linear regression modelling did not improve when the mutation coding DNA location was added a predictor (≤40 group p=0.76; >40 group p=0.35), nor with the addition of the ages of onset of subjective symptoms (nyctalopia and other visual symptoms) as predictors (≤40 group p=0.30; >40 group p=0.62).

There was a strong correlation (Spearman r=0.76) between the VA of both eyes in affected males (Fig. 3-10). This data was heteroskedastic, with higher variability at lower VA. Very poor VA in one eye (*e.g.*, worse than 1.0 logMAR (Snellen 20/200)) did not necessarily correspond with similar poor acuity in the fellow eye.

Visual Fields

The VF from the better eye of 64 different affected males were grouped by age and the modified "inclusion/exclusion" test was applied to determine the critical age for VF (Table 3-2; Fig. 3-11). The 21-30 subgroup was not significantly different from either the younger ≤20 grouping or the >30 group. Linear regressions were calculated with the critical ages of 20 and 30 to determine which model best fits the change in VF. With only the age of the males as a predictor, the coefficients of determination were R^2=0.264 (critical age: 20) and R^2=0.201 (critical age: 30), thus the VF critical age was defined as 20 years old.

Linear regression modelling (Fig. 3-12) predicted that the rate of change in the VF of males ≤20 years old was not significantly different from 0 (p=0.79). The rate of change of VF in males >20 years old was -0.868 horizontal degrees/year (p=0.006).

Individuals who were predicted to lack any *CHM* transcript or REP-1 protein fragments (due to whole gene deletions or deletions spanning the ATG start codon on exon 1) showed the same variability as the other *CHM* mutations. There was also no difference in the rate of decline in individuals with missense *CHM* mutations.

Multivariable linear regression modelling did not improve when the mutation cDNA location was added as a predictor (≤20 group p=0.68; >20 group p=0.72) nor with the addition of the age of onset of nyctalopia as a predictor (≤20 group p=0.80; >20 group p=0.96). The addition of the age of onset of other visual symptoms as a predictor significantly improved the model above the critical age (≤20 group p=0.80; >20 group p=0.0004). This multivariable model predicted that above 20 years of age, affected males' VF declined by 1.224 horizontal degrees/year (Fig. 3-13). Every year that affected males were free from symptoms of visual loss other than nyctalopia (*e.g.*, constriction of peripheral VF) corresponded with increased VF (1.228 horizontal degrees/symptom free year).

There was a very high correlation (Spearman r=0.95) between the VF of both eyes in affected males (Fig. 3-14). The correlation was consistent in both the early and late stages of choroideremia.

Longitudinal Analyses

Visual Acuity

The VA of 12 affected males were further analyzed using clinical data from repeated visits. The number of VA recorded for each individual ranged from 2 to 15 (mean=5.5

visits). Linear regressions were calculated for each individual as the small sample size precluded mixed model regression analysis for the entire sample (Fig. 3-15). No precipitous decline in vision was observed in any of the individuals, so all of the individuals were compared to the ≤40 group from the cross-sectional analysis. The mean rate of change for the longitudinal population was 0.00870 logMAR units/year. The 95% confidence interval of 9 individuals was not significantly different from 0 (the other 3 individuals had only 2 visits recorded and no confidence interval could be calculated). Thus, the longitudinal analysis showed that VA was stable in younger individuals with CHM and corroborated with the cross-sectional analysis.

Visual Fields

Repeated VF (2 or 3 visits) were recorded on 5 individuals above the age of 20 years old and linear regressions were calculated (Fig. 3-16). Visits prior to the critical age of 20 were excluded due to insufficient data for linear regressions. The mean rate of change observed was -1.58 horizontal degrees/year. With the exception of one outlier, the longitudinal data also corroborated with the rate of change observed in the cross-sectional sample.

Clinical tests

Full-field Stimulus Threshold

Eight males (ranging from 15 to 63 years old) underwent full-field stimulus threshold (FST) testing. A representative output showed the significant declines in threshold sensitivities for all stimuli in affected males (Fig. 3-17). Despite the decreased threshold

sensitivities, affected males were able to complete the testing with similar reliability and repeatability compared to the normal reference population.

Decreases in threshold sensitivities could be detected as early as 15 years of age and progressed in a semilog manner (Fig. 3-18). The threshold sensitivity to a white stimulus decreased at a faster rate when compared to red or blue stimuli; the threshold sensitivities to red and blue stimuli decreased at similar rates.

The calculated difference between red and blue threshold sensitivities represents the relative contribution of cone and rod populations [104, 107]. If the FST is >20 dB more sensitive to blue light than red light, it indicates that the response is primarily the result of rod photoreceptor activity. Conversely, if the red-blue difference is <3dB (or if the FST is more sensitive to red light), then cone photoreceptors are the primary contributors. Red-blue sensitivity differences >3 dB and <20 dB indicate that there is mixed rod-cone contribution to the detection of stimuli. Two males with CHM demonstrated purely cone-mediated perception, whereas the other six individuals had rod-mediated perception or were on the cusp between rod-mediated and mixed rod-cone mediated perception (Fig. 3-19).

Microperimetry

Representative microperimetry maps show the functional retinal islands of 40 year old and 63 year old males with choroideremia (Fig. 3-20). The 20° grid, shown in panel A, tests 41 stimuli in 5 concentric circles in addition to a central fovea stimulus, whereas the custom 11×11/20° grid tests a square pattern with 121 stimuli centered around the fovea. The 41 stimuli pattern was performed more quickly (testing duration: 4 min 50

sec) than the 121 stimuli grid (testing duration: 9 min 55 sec), but did not delineate the exact border and size of the functioning retinal island.

The microperimetry changes corresponded with the changes observed with Goldmann perimetry. However, the maximum grid size of 20° could not identify the outer borders of younger males who had visual fields greater than 20°.

Discussion

CHM Mutations

The frequency of *CHM* mutations in this study, particularly the skewed ratio of nonsense to missense mutations (Fig. 3-1), corresponds with previous reports and mutation databases. Along with the increased rate of nonsense mutations, a relative increase in the proportion of frameshift mutations resulting in premature truncation of *CHM* mRNA was also observed. This is an uncommon phenomenon in the human genome, as missense mutations are detected more frequently as disease causing mutations [118]. However, nonsense mutations are more commonly found in genes encoding for GTPase regulators, including *CHM*, *KRIT1* (which encodes for Krev interaction trapped-1), and *RPGR* (which encodes for X-linked retinitis pigmentosa GTPase regulator) [119]. It is not clear why specific classes of genes (such as the aforementioned GTPase regulators or tumour suppressor genes) have high proportions nonsense mutations, but it may reflect how missense mutations effect phenotypes and a result, bias the detection of mutations towards prematurely truncating mutations.

Several scenarios may explain the skewed mutation frequencies in *CHM*/REP-1. For example, missense mutations may cause such mild effects in REP-1 activity that they are not brought to clinical attention and instead reported as benign SNPs. There are 43 *CHM* missense variants reported in the Database of Single Nucleotide Polymorphisms (dbSNP; National Center for Biotechnology Information, National Library of Medicine. Bethesda, MD. dbSNP Build ID: 138) that have been detected with large scale

sequencing projects. Unfortunately, these large projects lack corresponding clinical data, so it is difficult to ascertain whether these variants are truly benign variants or individuals are presymptomatic males or CHM carriers. Conversely, missense mutations may have a dominant-negative phenotype if non-functional REP-1 binds unprenylated Rab proteins and inhibits any compensatory prenylation activity by REP-2. This could cause a severe phenotype such as the early death observed in *CHM*$^{-/-}$ zebrafish that lack a compensatory copy of rep-2 [78]. This mechanism is seen in other genes encoding for multimeric proteins (*e.g.*, *RYR3* encoding for Ryanodine receptor 3 [120]), but given that REP-1 functions as a monomer, this dominant negative phenomenon is less likely. A third alternative is that missense mutations cause a completely unrelated phenotype to CHM and, as a result, have yet to be associated with the *CHM* gene.

The HGMD database should also be viewed cautiously as a true representation of the frequency of pathogenic mutations in the human genome. While the HGMD was founded with the intention of documenting only mutations with confirmed pathogenic effects, inherent difficulties in undertaking such a monumental task have meant that the HGMD includes disease-causing mutations, potentially disease-causing mutations, as well as disease associated-polymorphisms that may or may not have functional evidence to support their inclusion in the HGMD [118]. Analysis of 1000 exomic sequences showed that only 7% of unique variants flagged by the HGMD were actually pathogenic after in-depth review [121]. Thus, a significant portion of the missense mutations reported in the database may not represent true pathogenic mutations and, as a result, the HGMD overstates the rarity of pathogenic nonsense or prematurely truncating mutations.

The location of *CHM* mutations is also skewed: a cluster of mutations occurs in the region spanning c.701-800 and no pathogenic mutations are reported in the final 198 nucleotides (which makes up approximately 10% of the coding DNA in *CHM*) (Fig. 3-3). Mutation hotspots can be attributed to many characteristics of the DNA including the gene sequence, flanking regions, and secondary DNA structure (reviewed by Rogozin and Pavlov [122]). This study had 17 families with C>T mutations at 3 CpG dinucleotide loci resulting in premature stop codons. High rates of methylation at CpG dinucleotides and subsequent deamination resulting in a mutated TpG dinucleotide (changing a CGA-Arginine codon into a TGA-Stop codon) may account for why so many unrelated families have the same mutation at this location. Alternatively, the independent families may actually be distantly related, reflecting a weakness in this database review, and this finding is a spurious result. The least likely explanations for this mutation hotspot are based on the function of the mutated REP-1 protein. For example, should mutations from c.701-800 result in relatively high pathogenicity, they could cause a more severe phenotype and are brought to clinical attention more than other *CHM* mutations. This is unlikely given the lack of REP-1 expression precluding different levels of pathogenicity and this study's results showing that individuals harbouring these mutations exhibit the same phenotypic variability and severity as other *CHM* mutations.

The lack of pathogenic mutations near the 3' end of *CHM* may reflect that the terminal 3' nucleotides have a lower rate of mutagenesis relative to the rest of the gene. Alternatively, the absence of pathogenic mutations in exon 15 may reflect that the C-terminus tail may not be essential for REP-1 function, thus mutations are not identified

in the CHM population. The distal 47 residues form a flexible tail anchored by a chain of 4 proline residues (poly-P tail) and do not have a defined structure in crystallography or *in silico* modelling of the rat REP-1 protein [55-57]. The amino acid residues distal to the poly-P link are not conserved between species, suggesting that there is less evolutionary pressure on that part of the protein. Furthermore, any prematurely truncating mutations located in exon 15 of *CHM* may not result in NMD, as premature stop codons in the last exon can escape NMD at a relatively high rate [123]. Thus, REP-1 would still be expressed and be able function, albeit without a full-length poly-P tail. Unpublished data from Seabra suggested that the 70 C-terminal amino acid residues are obligatory for the proper function of REP-1 and prenylation of Rab proteins [124]. However, this truncated REP-1 would have lacked 22 amino acids upstream of the poly-P motif that are part of the defined structure of REP-1, which may be critical for Rab prenylation. Modelling by Rak *et al.* suggested that the C-terminal tail serves to protect the hydrophobic pocket that REP-1 in the absence of geranylated Rab proteins, allowing for the solubilization of REP-1 protein [56]. As long as the C-terminal tail is long enough to perform this function, truncating mutations may be silent. Thus, the lack of mutations near the 3' end of *CHM* and the obligatory presence of the 70 C-terminus residues are not mutually exclusive.

Missense Mutations

The novel missense mutations in this study (p.Gln273His, p.Leu457Pro, and p.Leu80Phe/p.Met443Val) have not had any protein expression or prenylation activity assays, which limits analyses of their effect on REP-1 to predictions based on *in silico* REP-1 modelling. REP-1 has been described as a two domain structure: domain I forms

the Rab binding platform (RBP) and is responsible for the association and positioning of Rab proteins in the REP-1:Rab:GGTase-2 complex; domain II is responsible for the association of GGTase-2 necessary for prenylation activity [54, 125]. Domain I is made up of 6 α-helixes and 4 β-sheets and domain II is formed by 5 α-helixes [55]. The p.Gln273 residue is part of β-sheet b2, which links the domain II helixes to domain I and creates a pocket for GGPP. Functional predictions of substituting a histidine residue for glutamine are equivocal: PolyPhen-2 predicted that the mutation is probably damaging, whereas the SNAP tool predicted that the substitution is neutral. The HSF tool predicted that the c.819G>T substitution causing this mutation would probably affect splicing, as it occurs within the donor site of exon 6. Experimental confirmation is necessary to determine whether the *CHM* mRNA transcript is appropriately spliced and, if the mRNA transcript is full-length, whether REP-1$^{p.Gln273His}$ is translated into a full-length protein that is able to fold into the correct REP-1 tertiary structure. Given the role of glutamine in maintaining the GGPP pocket, changes in the local microenvironment could alter REP-1 prenylation activity to render REP-1$^{p.Gln273His}$ non- or hypofunctional, causing CHM despite adequate REP-1 expression.

The p.Leu457Pro mutation is located within a β-sheet in domain I and both of the PolyPhen-2 and SNAP programs predict that the mutation will be damaging to REP-1. The introduction of a kinked proline residue into an organized β-sheet will cause disruption of the tertiary structure which potentially results in a loss-of-function or degradation of the mutated REP-1 protein. A mutated REP-1$^{p.Leu550Pro}$ protein, which also substitutes a proline for a leucine located in a β-sheet in domain I, has been modelled *in*

silico and undergone *in vitro* Western blot confirmation that the mutation causes very low REP-1 expression [57]. The low REP-1$^{p.Leu550Pro}$ expression reported by Sergeev *et al.* can be attributed to destruction of aberrantly formed proteins by the unfolded protein response (UPR) [63].

Both p.Leu80 and p.Met443 residues are located in α-helixes within domain I. The p.Leu80Phe and p.Met443Val substitutions are predicted to be conservative with no functional effect by both PolyPhen-2 HumVar and SNAP. The p.Leu80Phe mutation has been reported as a SNP in a paper demonstrating a novel sequencing technique [126]. The source DNA was from 2 individuals: a Mormon female from Utah and a Yoruba male from Ibadan, Nigeria with no CHM phenotype, but it is not described which proband carries the REP-1$^{p.Leu80Phe}$ mutation. The affected individual may truly lack a CHM phenotype, but it's also possible that, depending on who carries the mutation, CHM was not diagnosed in the female carrier or the male was pre-symptomatic (depending on his age). Alternatively, these two mutations could be neutral (or cause subclinical REP-1 hypofunction) in isolation, but when combined together, the REP-1 dysfunction is more severe and results in the CHM phenotype. HSF predicted potential alterations of splicing through alteration of silencer and enhancer motifs as well as the generation of a potential cryptic donor site in exon 10. A third explanation could be that these two variants are truly benign and a third, undetected pathogenic mutation is responsible for the subject's CHM phenotype. If this putative third mutation were located deep within a large intron, it may not have been sequenced as the large size of *CHM* introns precludes sequencing them in their entirety and only limited number of nucleotides are

sequenced at the intron-exon junctions; likewise, if the third mutation was located in a regulatory sequence outside of the *CHM* gene, it may also have been missed in the genotyping process. The two detected variants may be in linkage disequilibrium with the third mutation and appear to segregate with the phenotype when the family is genotyped, but in fact be harmless variants. Studies of mRNA transcripts and protein expression or function would be pertinent to investigate the impact of these two *CHM* mutations.

Ultimately, further investigation of these missense mutations is required to fully characterize their effect on REP-1 and Rab prenylation. Northern blot assays to determine mRNA length, combined with cDNA sequencing of mature mRNA, would be able to detect any alternative splicing. Western blot assays to ascertain expression levels of mutated REP-1 would establish whether there is any protein degradation via the UPR. Should any REP-1 be expressed, prenylation assays for activity and interaction studies of the REP-1:Rab:GGTase2 complex formation could shed light on the molecular pathogenesis of CHM given the paucity of expressed mutated REP-1 proteins.

Natural History of CHM

Subjective Symptoms

The onset of subjective symptoms of nyctalopia or other visual loss was at 12.6 and 19.7 years of age, respectively, which agrees with previously published descriptions of CHM [2]. The degenerative process of CHM likely begins at birth (evidenced by the early changes observed with OCT and other testing modalities), but the loss of rod photoreceptors and

resultant nyctalopia may be underreported due to the young age of affected males. In order to report their symptoms to a parent or ophthalmologist, affected individuals must be able to infer that their dark adapted vision is inferior to peers and articulate this to their parents. Likewise, other visual loss (*i.e.*, constriction of VF) can be detected using perimetry testing at younger ages, but is not self-reported until the VF loss is moderately advanced and impinging on activities in a noticeable manner. The age of onset of visual field loss also corresponded with the critical age for VF changes (calculated to be 20 years old) based on the cross-sectional analysis. A precipitous decline in the width of the VF was observed at 20 years of age, confirming the accuracy of self-reported symptoms. Self-reported symptoms have limitations, especially in retrospective studies – patients can have recall biases, affirmation biases (where asymptomatic individuals agree with physician questions), or misclassification of responses (*e.g.* it is unlikely that a male would experience the onset of nyctalopia and other visual symptoms at 50 years of age, nor would a 1 year old infant be able to report any symptoms). However, in this study, responses agreed with previous observations and the other results in this study, demonstrating external and internal validity.

Visual Acuity

In the cross sectional analysis, the VA of affected individuals was stable until 40 years of age, after which there was a variable decline in VA at an average rate of 0.0483 logMAR units/year. The longitudinal analysis corroborated with the cross-sectional results (albeit with the caveat of a small sample size), demonstrating a statistically insignificant decline in VA that was also observed in the ≤40 cohort. The rate of change in the >40 group is

approximately 2.5× larger than the 0.018 logMAR units/year rate reported by Roberts *et al.* [4]. However, Roberts' rate was derived from longitudinal data which included affected males from 6 to 66 years of age, so it reflected the life-long changes in VA observed in CHM and could not be directly compared to the biphasic model used in this study. Further, 93% of Roberts' sample had rates of change below 0.018 logMAR units/year, indicating that the data was skewed heavily towards a slower rate of change, which is what one would expect given that declines in VA were observed in those >40 years of age (only 22% of Roberts' sample was older than 40 years of age). Coussa *et al.* calculated a critical age of 50 years in their cross-sectional analysis and found there was no significant change in VA below 50 years of age, but the rate of change of VA is 0.0206 logMAR units/year for males >50 years old [5]. This is less than our observed rate and may reflect the Coussa's use of a different critical age and methodological differences in analysis. Methodological differences include the use of different definitions of CF, HM, LP, and NLP VA, as well as the inclusion of multiple data points from individuals and fellow eyes without any statistical correction for the lack of independence between data points.

The dramatic drop in VA above 40 years of age can be attributed to the advancing RPE degeneration (and shrinking borders of the island of surviving retinal photoreceptors) impinging on the foveola and the eventual disruption of the fovea. The longitudinal cohort did show gradual declines in their VA, which may reflect a combination of nuclear and posterior subcapsular lens opacification and intraocular light scatter associated with advanced CHM, as well as decreased foveal sensitivity

observed in affected males prior to loss of foveal/foveolar photoreceptors [18, 19, 108]. Furthermore, this study design did not account for any co-morbid ocular conditions such as cystoid macular edema or other retinal pathologies that may disproportionately contribute to the VA changes observed in such a small sample [127].

Visual Fields & Microperimetry

The VF of affected individuals decreased at a linear rate of -0.868 to -1.224 horizontal degrees/year above the age of 20 years in both the cross-sectional and the longitudinal cohort. The rapid decline observed at 20 years of age is likely a true representation of the natural history of CHM as a similar decline had been previously observed in Goldmann VF quantified by Esterman scores [8]. Individuals less than 20 years of age had significant variability that may simply demonstrate interindividual variability, but may also reflect the difficulty in performing accurate perimetry in children combined with errors in measuring the width of VF. When the Goldmann VF outputs were included within the database files, the width of the continuous horizontal meridian was measured and calculated. However, many of the VFs were analyzed by the physician who submitted the patient data to eyeGENE™ and could not be assessed for accuracy. VF do not decrease in a regular pattern, reflecting that RPE and photoreceptor loss can progress irregularly with invaginations into the intact retinal island that are not accurately quantified by the horizontal meridian of the VF. Thus, young individuals may have large VF that extend beyond the physiologic blind spot or have scotomas that impinge on the meridian. These instances may result in inconsistent measurement of

the horizontal meridian with no possibility of confirming the VF measurement to ensure compliance with the study methodology.

There has been no universally adopted technique for quantification of Goldmann VF, likely due to the wide variety of diseases that are assessed by Goldmann VF and have their own characteristics that preclude a single standardized grading technique. For example, neuro-ophthalmological deficits often present in stereotypical patterns that are best described in a qualitative manner (*e.g.,* nasal step, hemianopia respecting vertical meridian, *etc.*) whereas hereditary diseases such as choroideremia and retinitis pigmentosa that present with a progressive, concentric constriction of VF can be described by quantifying the remaining VF [128, 129]. Multiple quantification measures have been implemented to quantify Goldmann VF: Esterman scores using a grid system to grade the VF, measuring the diameter of VF across a single dimension (used in this study), and quantification of VF areas using planimetry [129, 130]. However, these techniques have been supplanted by computerized measurement of VF areas, which is more accurate and repeatable compared to older methods (but requires access to the source data, which was unavailable in this study) [131]. Whether the measured area includes a physiologic or enlarged blind spot, and/or non-contiguous islands of vision needs to be standardized to allow for accurate follow-up of patients in clinical trials and allow for comparison between studies. Furthermore, the size and intensity of stimuli used in Goldmann perimetry is often at the discretion of the ophthalmologist or perimeter operator, which introduces another dimension of variability into analysis. Again, a standard needs to be established with specific stimuli being used in all

individuals' perimetry testing to allow for accurate comparison among individuals. In severe hereditary retinopathies such as CHM or RP, the minimum standard should include the V4e stimulus as this is the largest and brightest stimulus and can be used to establish the maximum size of the VF and quantify visual function in very low vision populations [132]. Smaller or dimmer stimuli (even the III4e stimuli that is most commonly used) are less useful in moderate to advanced stages of CHM because the isopters they delineate quickly become too small to document any disease progression (if they can even be detected by very low vision patients). An effort should be made through international committees, such as the Imaging and Perimetry Society, to clarify existing standards and expand on the optimal techniques and analysis to guide researchers and clinicians using perimetry in hereditary retinopathies such as CHM [133].

A significant limitation of Goldmann perimetry is the lack of spatial resolution, particularly in advanced CHM where VFs are extremely constricted. In individuals with VF less than 20° in diameter, microperimetry can reliably and accurately quantify VF using static stimuli. As demonstrated in this study, microperimetry parameters must be optimized in order to generate useful and repeatable results. The standard 41 stimuli grid organized in a spoke pattern was insufficient to define the precise borders of retinal islands, which is a critical feature of microperimetry that will identify positive or negative responses to gene therapy or other future clinical trials in the treatment of CHM. However, the 121 stimuli pattern organized in an 11×11 grid can accurately define retinal islands with a resolution of 2° with the drawback of prolonged testing times. Using the '4-2 step' testing protocol, the microperimeter tests each stimulus location

multiple times, which can slow down the test significantly when the stimuli are outside of the patients' field of vision or within an area of absolute scotoma. The addition of a 'scotoma finder' protocol can expedite this testing process: by only using the maximal stimulus intensity for each of the 121 points on the grid, the microperimeter can quickly establish areas of absolute scotoma and the borders of the retinal island. The operator can shorten subsequent tests by removing extraneous test points beyond the borders of the retinal island (while still maintaining an appropriate margin of test points around the island in case there is expansion of the retinal island after therapy). By starting with the 'scotoma finder' protocol on the 121 stimuli grid and then performing the '4-2 step' protocol on the modified (<121 stimuli) grid, a balance between testing duration and useful microperimetry results can be found. The reduced testing duration minimizes patient fatigue or discomfort, increasing compliance during testing of the fellow eye and at follow-up visits.

As an adjunct test, FAF may serve as an additional biomarker for VF by quantifying the progression of RPE degeneration [108, 134]. The hyperfluorescence of the retinal island in FAF can be easily measured and quantified without the errors associated with the subjective perimetry responses.

Full-field Stimulus Threshold

The dark-adapted sensitivities of affected males were reduced with increased age, suggesting that FST can serve as a quantifiable marker of retinal function in CHM. Curiously, the rates of change in threshold sensitivities were not statistically significantly different between the different colour stimuli. Given the early onset of nyctalopia and

significant peripheral degeneration resulting in loss of rod photoreceptors, it was hypothesized that this would be reflected in a faster decrease in the threshold sensitivity to blue stimuli. However, this study found that the sensitivity to white stimuli decreased at the fastest rate and the sensitivities to red or blue stimuli both decreased at similar rates. This equal rate of decline was reflected in the red-blue threshold sensitivity difference: 75% of the tested males (6/8 males; ranging from 15 to 63 years old) were clustered around the border of the normal reference range (normal > 20 dB) and did not show cone-dominated responses. This surprising result may reflect separate processes in the cone and rod photoreceptor populations.

The threshold sensitivity to red stimuli should only reflect activation of cone photoreceptors (based on the spectral sensitivities of the L- and M-cones compared to rod photoreceptors) and its unexpected reduction suggests that cone photoreceptor function is affected early in the course of CHM, even while central VA is maintained. This surprising finding of cone dysfunction is supported by microperimetry reports of loss of foveal sensitivity in affected males, which also demonstrates that cone photoreceptors are affected early in the course of CHM [108]. These changes in foveal sensitivity observed with microperimetry precede the critical age when central VA begins to decline. Foveal sensitivity assessed by microperimetry can also identify macular changes earlier than VA or low-luminance VA in AMD, as well as subclinical changes in female carriers of CHM [24, 135]. Thus, with further study of longitudinal changes using microperimetry and FST, one may be able to predict which males with CHM are at higher risk of central VA decline

(based on the degree of loss of central retinal sensitivity or cone sensitivity to red stimuli).

The preservation of the red-blue threshold sensitivity difference may also reflect a relative conservation of rod photoreceptor function, despite a disproportionately large loss of the rod photoreceptor population. The relative loss of rods compared to cones may be underestimated by the FST test, as rods are sensitive to single photon stimulation [136]. Combined with post-synaptic convergence, this may be sufficient to generate a better threshold sensitivity than might otherwise be expected based on the number of surviving rod photoreceptors (particularly under these controlled experimental conditions). Alternatively, the red light stimulus may overlap with the spectral sensitivity of rods enough to prevent differentiation of the rod and cone responses in CHM. Nevertheless, 25% (n=2) of the individuals with advanced CHM had threshold sensitivities that were cone-dominated (as initially predicted); further testing of the CHM males is necessary to determine the natural history with respect to FST.

The FST can serve as a useful marker of dark-adapted retinal function and represents improvement on previous tests of dark adaptation, such as dark adaptometry. The repeatability of the test results is better than standard dark adaptometry: the between-visit coefficient of variation of FST with white stimuli ranged from 7.1% to 9.6%; with blue stimuli, 5.3% to 16.1%; and with red stimuli, 0.2% to 6.4%. In comparison, the coefficient of variation for standard dark adaptometry tested in severe eye disease was approximately 20% [137]. The improved coefficient of variation of

FST will decrease the error in follow-up visits in clinical trials, allowing for detection of statistically significant changes earlier than if standard dark adaptometry is used.

Genotype-Phenotype Correlations

There were no genotype-phenotype correlations or associations identified by this study for symptom onset, change in VA, or VF. This conclusion is based on the statistical analysis of the location of mutations along *CHM* cDNA. As well, a qualitative analysis of the CHM phenotypes caused by missense mutations compared to those due to absent REP-1 protein (due to whole gene deletions or the lack of an ATG start codon) and those with to nonsense mutations did not reveal any trends or patterns consistent with a genotype-phenotype relationship (Figs. 3-6, 3-9 and 3-12). The absence of any genotype-phenotype correlations can be attributed to the lack of detectable REP-1 expression (or extremely low levels of non-functional REP-1) resulting in a uniform decrease in the prenylation activity in affected males, regardless of the *CHM* mutation. The lack of protein expression in missense mutations may stem from NMD, UPR, or the previously discussed regulatory mutations in linkage disequilibrium that eliminate any protein expression. The phenotypic variability in CHM may result from a combination of other less understood contributors, such as environmental factors (*e.g.*, ultraviolet light exposure [138], nutrition [139], concomitant statin use [140, 141], *etc.*), other genetic factors (*e.g.*, epistatic effects from polymorphisms in genes/proteins associated with REP-1 prenylation), or stochastic effects. Theoretically, should a subset of individuals with hypo- or loss-of-function mutations in REP-2 (which could be compensated for by REP-1) be unmasked by REP-1 null mutations, individuals may undergo faster or more severe

degeneration. This has not been demonstrated in an affected individual, nor have any clinically significant *CHML* mutations been detected. The low prevalence of CHM and large number of unique *CHM* mutations means that population studies to assess risk factors are difficult to perform with sufficient statistical power to discover any subtle genotype-phenotype relationships. As a result, *in vitro* or *in vivo* studies will likely be the sources of additional information for insight into phenotypic variability.

Implications for Clinical Management & Clinical Trials

This study describes several important aspects of the natural history of CHM (*i.e.*, VA, VF, FST, and microperimetry) that are pertinent to management and counselling for the disease, particularly in the upcoming era of ocular gene therapy. By describing the observed changes in VA and VF in a large cross-sectional sample, counselling of affected individuals can include important descriptors such as the critical ages for changes in VA and VF, as well as the rate of changes in VA and VF. In addition to improved counselling of CHM patients, these results can be applied to the selection of participants for gene therapy trials for CHM.

Selection of individuals for early clinical trials in Phase I or Phase I/II is critical in order to adequately demonstrate the safety of the intervention, as well as maximize the ability of researchers to demonstrate efficacy (over an appropriate time period). Ethically, one must balance the fact that unproven treatments in clinical trials should be reserved as a last-resort (*i.e.*, older, more severely affected individuals are typical candidates for Phase I trials) while considering that a key determinant in the success of a clinical trial of CHM gene therapy will be the number of surviving photoreceptor and

RPE cells being treated (*i.e.*, favouring the enrolment of younger individuals) [142]. This is a difficult ethical issue to balance the risks and benefits of the trial that must be addressed with prospective participants and a thorough informed consent is necessary. One must also consider the participant characteristics carefully so that study goals can be achieved: it would be unethical to subject participants to an experimental and potentially dangerous treatment if their disease characteristics precluded the demonstration of safety or efficacy due to floor or ceiling effects. For example, should a participant with advanced CHM who has HM VA suffer an adverse event from the surgical intervention, very little change in VA could be observed, which would mask the severity of the adverse event.

When considering how to demonstrate efficacy of the treatment, one must consider that treated individuals who are very young may not show any effect for decades as photoreceptors and RPE outside the treated area would continue to degenerate at a predictably slow rate. VA would not be a differentiating test, nor would Goldmann perimetry, as both tests would likely be unchanged until late in the disease course. At the other extreme, individuals with end-stage CHM would be poor candidates to demonstrate efficacy, as there would be very few remaining photoreceptors or RPE cells to transfect and rescue. Thus, outcome measures would likely continue to be very poor with little observable change to differentiate successful therapy from failure.

The optimal individual for a CHM gene therapy trial would be on the cusp of degeneration of central acuity and have symmetric VA, VF (including microperimetry), and FST results. In this individual, a successful treatment would show preservation (or

even improvement) of outcome measures in the treated eye, whereas the untreated fellow eye would continue to deteriorate. Symmetry of the eyes (at time of enrolment) is critical, as gene therapy trials cannot be implemented in a randomized, placebo-controlled manner, so the untreated fellow eye serves as an important comparator to assess the efficacy of gene therapy. Age is the only predictor of the decline in VA, so participants who are older than the critical age of 40 years old are at a higher risk of degeneration and should be selected. In order to demonstrate preservation of VA, individuals should have good acuity at baseline (*e.g.,* better than 20/50 OU). The visual fields of participants should be large enough to be reliably reproduced with microperimetry, as well as have sufficient size that the borders of the retinal island aren't impinging on the central foveal area. The retinal island should also be smaller than approximately 15° in diameter so it can be followed with microperimetry (with a margin to allow for any potential expansion of the retinal island). This VF criterion would exclude most individuals below 40 years of age or above 60 years of age. FST and FAF can be performed reliably in nearly every individual, but participants should be tested to ensure they can comply with the testing protocols and appropriate results are obtained. Other traditional testing modalities such as dark adaptometry or ERGs are not sensitivity or reliable enough in the CHM population and their role should be limited to use as supplementary tests. *CHM* mutations should be confirmed via direct sequencing, but no preference should be given to a particular mutation, as there are no genotype-phenotype correlations in CHM. These criteria would minimize the follow-up time necessary to show any improvement because there would be sufficient photoreceptor

and RPE tissue to be rescued, as well as the untreated eyes would be at the highest risk VA deterioration and have further loss of VF (compared to the treated eye).

Conclusions

CHM is a debilitating diagnosis for affected individuals due to its intractable degeneration with an unpredictable natural history. Patient counselling has been limited to knowledge gleaned from small case series and studies that lack the sample size or new diagnostic tools (such as FST or microperimetry). These studies also lack any analysis of patients' *CHM* genotype in relation to their phenotypes. This study addresses these gaps in the knowledge of the natural history of CHM by describing the changes in VA and VF in a quantified and clinically relevant manner. Establishing critical ages for individuals with CHM, as well as defining the rates of change in VA and VF, provides valuable information to ophthalmologists treating affected males. This new data can also guide ophthalmologists when discussing the natural history of CHM with patients, creating more accurate expectations in their patients about how their disease will progress over time. Furthermore, this study provides the strongest evidence to date against any genotype-phenotype correlations in CHM. Investigators undertaking studies of CHM, including clinical trials, may comfortably group all CHM males together to maximize their sample size and resultant statistical power.

The introduction of FST and microperimetry protocols for use in CHM will also be relevant in both the clinic and research settings. FST testing is able to more accurately and reliably quantify the degree of nyctalopia in males compared to traditional techniques such as dark adaptometry. The novel feature of quantifying the relative contributions of the rod and cone photoreceptors needs further study, but may also

provide valuable data on how rod and cone photoreceptor populations degenerate and respond to gene therapy. The modifications to the standard microperimetry protocol that take into account the unique features and limitations of males with CHM allow the utility of the microperimeter to be maximized. Not only will microperimetry define the borders of retinal islands in the macula more accurately compared to standard Goldmann or Humphrey VF machines, it will also be able to test the exact same retinal points and track changes in retinal sensitivity in response to gene therapy. The modified protocol minimizes discomfort for the patient while maximizing the data collected by the microperimeter.

These improvements in describing the natural history of CHM, as well as novel techniques in assessing visual function, will provide valuable guidance for ophthalmologists caring for patients with CHM as well as investigators implementing clinical trials for the treatment of CHM.

References

1. Mauthner H. Ein fall von chorioideremia. Naturwissenschaftlich Medezinischer Verein 1871;2191.

2. MacDonald IM, Smaoui N, Seabra MC. Choroideremia. In: Pagon RA, Bird TD, Dolan CR, et al, eds. GeneReviews. Seattle (WA): University of Washington, Seattle; 1993.

3. van den Hurk JA, Schwartz M, van Bokhoven H, et al. Molecular basis of choroideremia (CHM): Mutations involving the rab escort protein-1 (REP-1) gene. Hum Mutat 1997;9(2):110-7.

4. Roberts MF, Fishman GA, Roberts DK, et al. Retrospective, longitudinal, and cross sectional study of visual acuity impairment in choroideraemia. British Journal of Ophthalmology 2002;86(6):658-62.

5. Coussa RG, Kim J, Traboulsi EI. Choroideremia: Effect of age on visual acuity in patients and female carriers. Ophthalmic Genet 2012;33(2):66-73.

6. Esposito G, De Falco F, Tinto N, et al. Comprehensive mutation analysis (20 families) of the choroideremia gene reveals a missense variant that prevents the binding of REP1 with rab geranylgeranyl transferase. Hum Mutat 2011;32(12):1460-9.

7. Karna J. Choroideremia. A clinical and genetic study of 84 finnish patients and 126 female carriers. Acta Ophthalmol Suppl 1986;1761-68.

8. Rosenberg T, Schwartz M. Age differences of visual field impairment and mutation spectrum in danish choroideremia patients. Acta Ophthalmol (Copenh) 1994;72(6):678-82.

9. Hirakawa H, Iijima H, Gohdo T, et al. Progression of defects in the central 10-degree visual field of patients with retinitis pigmentosa and choroideremia. Am J Ophthalmol 1999;127(4):436-42.

10. Renner AB, Kellner U, Cropp E, et al. Choroideremia: Variability of clinical and electrophysiological characteristics and first report of a negative electroretinogram. Ophthalmology 2006;113(11):2066,2073.e2.

11. Syed R, Sundquist SM, Ratnam K, et al. High-resolution images of retinal structure in patients with choroideremia. Invest Ophthalmol Vis Sci 2013;54(2):950-61.

12. Noble KG, Carr RE, Siegel IM. Fluorescein angiography of the hereditary choroidal dystrophies. Br J Ophthalmol 1977;61(1):43-53.

13. Chen MS, Chang CC, Ho TC, et al. Blood-aqueous barrier function in a patient with choroideremia. J Formos Med Assoc 2010;109(2):167-71.

14. Lazow MA, Hood DC, Ramachandran R, et al. Transition zones between healthy and diseased retina in choroideremia (CHM) and stargardt disease (STGD) as compared to retinitis pigmentosa (RP). Invest Ophthalmol Vis Sci 2011;52(13):9581-90.

15. Jacobson SG, Cideciyan AV, Sumaroka A, et al. Remodeling of the human retina in choroideremia: Rab escort protein 1 (REP-1) mutations. Invest Ophthalmol Vis Sci 2006;47(9):4113-20.

16. Genead MA, McAnany JJ, Fishman GA. Retinal nerve fiber thickness measurements in choroideremia patients with spectral-domain optical coherence tomography. Ophthalmic Genet 2011;32(2):101-6.

17. Itabashi T, Wada Y, Kawamura M, et al. Clinical features of japanese families with a 402delT or a 555-556delAG mutation in choroideremia gene. Retina 2004;24(6):940-5.

18. Grover S, Alexander KR, Choi DM, et al. Intraocular light scatter in patients with choroideremia. Ophthalmology 1998;105(9):1641-5.

19. Grover S, Alexander KR, Fishman GA, et al. Comparison of intraocular light scatter in carriers of choroideremia and X-linked retinitis pigmentosa. Ophthalmology 2002;109(1):159-63.

20. Huang AS, Kim LA, Fawzi AA. Clinical characteristics of a large choroideremia pedigree carrying a novel CHM mutation. Arch Ophthalmol 2012;130(9):1184-9.

21. Preising MN, Wegscheider E, Friedburg C, et al. Fundus autofluorescence in carriers of choroideremia and correlation with electrophysiologic and psychophysical data. Ophthalmology 2009;116(6):1201,9.e1-2.

22. Renner AB, Fiebig BS, Cropp E, et al. Progression of retinal pigment epithelial alterations during long-term follow-up in female carriers of choroideremia and report of a novel CHM mutation. Arch Ophthalmol 2009;127(7):907-12.

23. Vajaranant TS, Fishman GA, Szlyk JP, et al. Detection of mosaic retinal dysfunction in choroideremia carriers electroretinographic and psychophysical testing. Ophthalmology 2008;115(4):723-9.

24. Thobani A, Anastasakis A, Fishman GA. Microperimetry and OCT findings in female carriers of choroideremia. Ophthalmic Genet 2010;31(4):235-9.

25. Lyon MF. Gene action in the X-chromosome of the mouse (mus musculus L.). Nature 1961;190372-3.

26. Majid MA, Horsborough B, Gray RH. Unusual macular findings in a known choroideremia carrier. Eye (Lond) 1998;12 (Pt 4)(Pt 4):740-1.

27. Rudolph G, Preising M, Kalpadakis P, et al. Phenotypic variability in three carriers from a family with choroideremia and a frameshift mutation 1388delCCinsG in the REP-1 gene. Ophthalmic Genet 2003;24(4):203-14.

28. Syed N, Smith JE, John SK, et al. Evaluation of retinal photoreceptors and pigment epithelium in a female carrier of choroideremia. Ophthalmology 2001;108(4):711-20.

29. Flannery JG, Bird AC, Farber DB, et al. A histopathologic study of a choroideremia carrier. Invest Ophthalmol Vis Sci 1990;31(2):229-36.

30. Gordiyenko NV, Fariss RN, Zhi C, et al. Silencing of the CHM gene alters phagocytic and secretory pathways in the retinal pigment epithelium. Invest Ophthalmol Vis Sci 2010;51(2):1143-50.

31. Strunnikova NV, Barb J, Sergeev YV, et al. Loss-of-function mutations in rab escort protein 1 (REP-1) affect intracellular transport in fibroblasts and monocytes of choroideremia patients. PLoS One 2009;4(12):e8402.

32. Sparrow JR, Hicks D, Hamel CP. The retinal pigment epithelium in health and disease. Curr Mol Med 2010;10(9):802-23.

33. Tolmachova T, Anders R, Abrink M, et al. Independent degeneration of photoreceptors and retinal pigment epithelium in conditional knockout mouse models of choroideremia. J Clin Invest 2006;116(2):386-94.

34. Strunnikova N, Zein WM, Silvin C, et al. Serum biomarkers and trafficking defects in peripheral tissues reflect the severity of retinopathy in three brothers affected by choroideremia. Adv Exp Med Biol 2012;723381-7.

35. MacDonald IM, Russell L, Chan C. Choroideremia: New findings from ocular pathology and review of recent literature. Surv Ophthalmol 2009;54(3):401-7.

36. Bonilha VL, Trzupek KM, Li Y, et al. Choroideremia: Analysis of the retina from a female symptomatic carrier. Ophthalmic Genet 2008;29(3):99-110.

37. Goldberg NR, Greenberg JP, Laud K, et al. Outer retinal tubulation in degenerative retinal disorders. Retina 2013;33(9):1871-6.

38. Zweifel SA, Engelbert M, Laud K, et al. Outer retinal tubulation: A novel optical coherence tomography finding. Arch Ophthalmol 2009;127(12):1596-602.

39. Leung KF, Baron R, Seabra MC. Thematic review series: Lipid posttranslational modifications. geranylgeranylation of rab GTPases. J Lipid Res 2006;47(3):467-75.

40. Wu Y, Goody RS, Abagyan R, et al. Structure of the disordered C terminus of Rab7 GTPase induced by binding to the rab geranylgeranyl transferase catalytic complex reveals the mechanism of rab prenylation. Journal of Biological Chemistry 2009;284(19):13185-92.

41. Baron RA, Seabra MC. Rab geranylgeranylation occurs preferentially via the pre-formed REP-RGGT complex and is regulated by geranylgeranyl pyrophosphate. Biochem J 2008;415(1):67-75.

42. McCaffrey MW, Lindsay AJ. Rab family. In: Editors-in-Chief: William J. Lennarz, M. Daniel Lane, eds. Encyclopedia of Biological Chemistry. New York: Elsevier; 2004:629-34.

43. Seabra MC, Brown MS, Goldstein JL. Retinal degeneration in choroideremia: Deficiency of rab geranylgeranyl transferase. Science 1993;259(5093):377-81.

44. Handley MTW, Burgoyne RD. The Rab27 effector rabphilin, unlike granuphilin and Noc2, rapidly exchanges between secretory granules and cytosol in PC12 cells. Biochem Biophys Res Commun 2008;373(2):275-81.

45. Seabra MC, Ho YK, Anant JS. Deficient geranylgeranylation of ram/Rab27 in choroideremia. J Biol Chem 1995;270(41):24420-7.

46. Griscelli C, Durandy A, Guy-Grand D, et al. A syndrome associating partial albinism and immunodeficiency. Am J Med 1978;65(4):691-702.

47. Durmaz A, Ozkinay F, Onay H, et al. Molecular analysis and clinical findings of griscelli syndrome patients. J Pediatr Hematol Oncol 2012;34(7):541-4.

48. Wavre-Shapton ST, Tolmachova T, Lopes da Silva M, et al. Conditional ablation of the choroideremia gene causes age-related changes in mouse retinal pigment epithelium. PLoS One 2013;8(2):e57769.

49. Li W. Phagocyte dysfunction, tissue aging and degeneration. Ageing Research Reviews 2013;12(4):1005-12.

50. Cremers FP, Armstrong SA, Seabra MC, et al. REP-2, a rab escort protein encoded by the choroideremia-like gene. J Biol Chem 1994;269(3):2111-7.

51. Tanaka D, Kameyama K, Okamoto H, et al. Caenorhabditis elegans rab escort protein (REP-1) differently regulates each rab protein function and localization in a tissue-dependent manner. Genes Cells 2008;13(11):1141-57.

52. Schalk I, Zeng K, Wu SK, et al. Structure and mutational analysis of rab GDP-dissociation inhibitor. Nature 1996;381(6577):42-8.

53. Soldati T, Riederer MA, Pfeffer SR. Rab GDI: A solubilizing and recycling factor for rab9 protein. Mol Biol Cell 1993;4(4):425-34.

54. Alory C, Balch WE. Molecular evolution of the rab-escort-protein/guanine-nucleotide-dissociation-inhibitor superfamily. Mol Biol Cell 2003;14(9):3857-67.

55. Pylypenko O, Rak A, Reents R, et al. Structure of rab escort protein-1 in complex with rab geranylgeranyltransferase. Mol Cell 2003;11(2):483-94.

56. Rak A, Pylypenko O, Niculae A, et al. Structure of the Rab7:REP-1 complex: Insights into the mechanism of rab prenylation and choroideremia disease. Cell 2004;117(6):749-60.

57. Sergeev YV, Smaoui N, Sui R, et al. The functional effect of pathogenic mutations in rab escort protein 1. Mutat Res 2009;665(1-2):44-50.

58. Cremers FP, van de Pol DJ, van Kerkhoff LP, et al. Cloning of a gene that is rearranged in patients with choroideraemia. Nature 1990;347(6294):674-7.

59. Merry DE, Janne PA, Landers JE, et al. Isolation of a candidate gene for choroideremia. Proc Natl Acad Sci U S A 1992;89(6):2135-9.

60. van Bokhoven H, van den Hurk JA, Bogerd L, et al. Cloning and characterization of the human choroideremia gene. Hum Mol Genet 1994;3(7):1041-6.

61. Kervestin S, Jacobson A. NMD: A multifaceted response to premature translational termination. Nature Reviews Molecular Cell Biology 2012;13(11):700-12.

62. Schweingruber C, Rufener SC, Zund D, et al. Nonsense-mediated mRNA decay - mechanisms of substrate mRNA recognition and degradation in mammalian cells. Biochim Biophys Acta 2013;1829(6-7):612-23.

63. Cao SS, Kaufman RJ. Unfolded protein response. Current Biology 2012;22(16):R622-6.

64. Donnelly P, Menet H, Fouanon C, et al. Missense mutation in the choroideremia gene. Hum Mol Genet 1994;3(6):1017.

65. Beaufrere L, Claustres M, Tuffery S. No missense mutation in choroideremia patients analyzed to date. Ophthalmic Genet 1999;20(2):89-93.

66. Ramsden SC, O'Grady A, Fletcher T, et al. A clinical molecular genetic service for united kingdom families with choroideraemia. European Journal of Medical Genetics 2013;56(8):432-8.

67. Kozlowski P, Jasinska AJ, Kwiatkowski DJ. New applications and developments in the use of multiplex ligation-dependent probe amplification. Electrophoresis 2008;29(23):4627-36.

68. Chi JY, Macdonald IM, Hume S. Copy number variant analysis in CHM to detect duplications underlying choroideremia. Ophthalmic Genet 2013;34(4):229-33.

69. MacDonald IM, Mah DY, Ho YK, et al. A practical diagnostic test for choroideremia. Ophthalmology 1998;105(9):1637-40.

70. Garcia-Hoyos M, Lorda-Sanchez I, Gomez-Garre P, et al. New type of mutations in three spanish families with choroideremia. Invest Ophthalmol Vis Sci 2008;49(4):1315-21.

71. Cremers FP, Molloy CM, van de Pol DJ, et al. An autosomal homologue of the choroideremia gene colocalizes with the usher syndrome type II locus on the distal part of chromosome 1q. Hum Mol Genet 1992;1(2):71-5.

72. Hainrichson M, Nudelman I, Baasov T. Designer aminoglycosides: The race to develop improved antibiotics and compounds for the treatment of human genetic diseases. Org Biomol Chem 2008;6(2):227-39.

73. Bedwell DM, Kaenjak A, Benos DJ, et al. Suppression of a CFTR premature stop mutation in a bronchial epithelial cell line. Nat Med 1997;3(11):1280-4.

74. Barton-Davis ER, Cordier L, Shoturma DI, et al. Aminoglycoside antibiotics restore dystrophin function to skeletal muscles of mdx mice. J Clin Invest 1999;104(4):375-81.

75. Welch EM, Barton ER, Zhuo J, et al. PTC124 targets genetic disorders caused by nonsense mutations. Nature 2007;447(7140):87-91.

76. Wilschanski M, Miller LL, Shoseyov D, et al. Chronic ataluren (PTC124) treatment of nonsense mutation cystic fibrosis. Eur Respir J 2011;38(1):59-69.

77. Starr CJ, Kappler JA, Chan DK, et al. Mutation of the zebrafish choroideremia gene encoding rab escort protein 1 devastates hair cells. Proc Natl Acad Sci U S A 2004;101(8):2572-7.

78. Moosajee M, Tulloch M, Baron RA, et al. Single choroideremia gene in nonmammalian vertebrates explains early embryonic lethality of the zebrafish model of choroideremia. Invest Ophthalmol Vis Sci 2009;50(6):3009-16.

79. Moosajee M, Gregory-Evans K, Ellis CD, et al. Translational bypass of nonsense mutations in zebrafish rep1, pax2.1 and lamb1 highlights a viable therapeutic option for untreatable genetic eye disease. Hum Mol Genet 2008;17(24):3987-4000.

80. Goldmann T, Overlack N, Wolfrum U, et al. PTC124-mediated translational readthrough of a nonsense mutation causing usher syndrome type 1C. Hum Gene Ther 2011;22(5):537-47.

81. Goldmann T, Overlack N, Moller F, et al. A comparative evaluation of NB30, NB54 and PTC124 in translational read-through efficacy for treatment of an USH1C nonsense mutation. EMBO Mol Med 2012;4(11):1186-99.

82. Manuvakhova M, Keeling K, Bedwell DM. Aminoglycoside antibiotics mediate context-dependent suppression of termination codons in a mammalian translation system. RNA 2000;6(7):1044-55.

83. Auricchio A, Kobinger G, Anand V, et al. Exchange of surface proteins impacts on viral vector cellular specificity and transduction characteristics: The retina as a model. Hum Mol Genet 2001;10(26):3075-81.

84. Bett AJ, Prevec L, Graham FL. Packaging capacity and stability of human adenovirus type 5 vectors. J Virol 1993;67(10):5911-21.

85. Anand V, Barral DC, Zeng Y, et al. Gene therapy for choroideremia: In vitro rescue mediated by recombinant adenovirus. Vision Res 2003;43(8):919-26.

86. Lehrman S. Virus treatment questioned after gene therapy death. Nature 1999;401(6753):517-8.

87. Assessment of adenoviral vector safety and toxicity: Report of the national institutes of health recombinant DNA advisory committee. Hum Gene Ther 2002;13(1):3-13.

88. Maguire AM, Simonelli F, Pierce EA, et al. Safety and efficacy of gene transfer for leber's congenital amaurosis. N Engl J Med 2008;358(21):2240-8.

89. Bainbridge JW, Smith AJ, Barker SS, et al. Effect of gene therapy on visual function in leber's congenital amaurosis. N Engl J Med 2008;358(21):2231-9.

90. Jacobson SG, Cideciyan AV, Ratnakaram R, et al. Gene therapy for leber congenital amaurosis caused by RPE65 mutations: Safety and efficacy in 15 children and adults followed up to 3 years. Arch Ophthalmol 2012;130(1):9-24.

91. Weleber RG, Francis PJ, Trzupek KM. Leber congenital amaurosis. In: Pagon RA, Bird TD, Dolan CR, et al, eds. GeneReviews. Seattle (WA): University of Washington, Seattle; 1993.

92. Cideciyan AV, Jacobson SG, Beltran WA, et al. Human retinal gene therapy for leber congenital amaurosis shows advancing retinal degeneration despite enduring visual improvement. Proc Natl Acad Sci U S A 2013;110(6):E517-25.

93. Lebherz C, Maguire A, Tang W, et al. Novel AAV serotypes for improved ocular gene transfer. J Gene Med 2008;10(4):375-82.

94. da Cruz L, Coley BF, Dorn J, et al. The argus II epiretinal prosthesis system allows letter and word reading and long-term function in patients with profound vision loss. Br J Ophthalmol 2013;97(5):632-6.

95. Testa F, Maguire AM, Rossi S, et al. Three-year follow-up after unilateral subretinal delivery of adeno-associated virus in patients with leber congenital amaurosis type 2. Ophthalmology 2013;120(6):1283-91.

96. Tolmachova T, Tolmachov OE, Wavre-Shapton ST, et al. CHM/REP1 cDNA delivery by lentiviral vectors provides functional expression of the transgene in the retinal pigment epithelium of choroideremia mice. J Gene Med 2012;14(3):158-68.

97. Tolmachova T, Tolmachov OE, Barnard AR, et al. Functional expression of rab escort protein 1 following AAV2-mediated gene delivery in the retina of choroideremia mice and human cells ex vivo. J Mol Med (Berl) 2013;91(7):825-37.

98. Vasireddy V, Mills JA, Gaddameedi R, et al. AAV-mediated gene therapy for choroideremia: Preclinical studies in personalized models. PLoS One 2013;8(5):e61396.

99. MacLaren RE, Groppe M, Barnard AR, et al. Gene therapy for choroideremia - initial report on A new clinical trial. ARVO Meeting Abstracts 2012;53(6):5577.

100. van Driel MA, Maugeri A, Klevering BJ, et al. ABCR unites what ophthalmologists divide(s). Ophthalmic Genet 1998;19(3):117-22.

101. Genead MA, McAnany JJ, Fishman GA. Topical dorzolamide for treatment of cystoid macular edema in patients with choroideremia. Retina 2012;32(4):826-33.
102. Shinoda H, Koto T, Fujiki K, et al. Clinical findings in a choroideremia patient who underwent vitrectomy for retinal detachment associated with macular hole. Jpn J Ophthalmol 2011;55(2):169-71.
103. Zinkernagel MS, Groppe M, Maclaren RE. Macular hole surgery in patients with end-stage choroideremia. Ophthalmology 2013;120(8):1592-6.
104. Jacobson SG, Aleman TS, Cideciyan AV, et al. Defining the residual vision in leber congenital amaurosis caused by RPE65 mutations. Invest Ophthalmol Vis Sci 2009;50(5):2368-75.
105. Roman AJ, Cideciyan AV, Schwartz SB, et al. Intervisit variability of visual parameters in leber congenital amaurosis caused by RPE65 mutations. Invest Ophthalmol Vis Sci 2013;54(2):1378-83.
106. Klein M, Birch DG. Psychophysical assessment of low visual function in patients with retinal degenerative diseases (RDDs) with the diagnosys full-field stimulus threshold (D-FST). Doc Ophthalmol 2009;119(3):217-24.
107. Roman AJ, Schwartz SB, Aleman TS, et al. Quantifying rod photoreceptor-mediated vision in retinal degenerations: Dark-adapted thresholds as outcome measures. Exp Eye Res 2005;80(2):259-72.
108. Groppe M, Cottriall C, Downes S, et al. Correlation of retinal sensitivity with the area of normal auto-fluorescence in choroideremia patients. Invest Ophthalmol Vis Sci 2013;54(6):642.

109. Arnold K, Kiefer F, Kopp J, et al. The protein model portal. J Struct Funct Genomics 2009;10(1):1-8.

110. Krieger E, Darden T, Nabuurs SB, et al. Making optimal use of empirical energy functions: Force-field parameterization in crystal space. Proteins 2004;57(4):678-83.

111. Krieger E, Nielsen JE, Spronk CA, et al. Fast empirical pKa prediction by ewald summation. J Mol Graph Model 2006;25(4):481-6.

112. Adzhubei IA, Schmidt S, Peshkin L, et al. A method and server for predicting damaging missense mutations. Nat Methods 2010;7(4):248-9.

113. Bromberg Y, Rost B. SNAP: Predict effect of non-synonymous polymorphisms on function. Nucleic Acids Res 2007;35(11):3823-35.

114. Desmet FO, Hamroun D, Lalande M, et al. Human splicing finder: An online bioinformatics tool to predict splicing signals. Nucleic Acids Res 2009;37(9):e67.

115. den Dunnen JT, Antonarakis SE. Mutation nomenclature extensions and suggestions to describe complex mutations: A discussion. Hum Mutat 2000;15(1):7-12.

116. Stenson PD, Mort M, Ball EV, et al. The human gene mutation database: 2008 update. Genome Med 2009;1(1):13.

117. Schulze-Bonsel K, Feltgen N, Burau H, et al. Visual acuities "hand motion" and "counting fingers" can be quantified with the freiburg visual acuity test. Invest Ophthalmol Vis Sci 2006;47(3):1236-40.

118. Stenson PD, Mort M, Ball EV, et al. The human gene mutation database: Building a comprehensive mutation repository for clinical and molecular genetics, diagnostic testing and personalized genomic medicine. Hum Genet 2014;133(1):1-9.

119. Mort M, Ivanov D, Cooper DN, et al. A meta-analysis of nonsense mutations causing human genetic disease. Hum Mutat 2008;29(8):1037-47.

120. Dabertrand F, Morel JL, Sorrentino V, et al. Modulation of calcium signalling by dominant negative splice variant of ryanodine receptor subtype 3 in native smooth muscle cells. Cell Calcium 2006;40(1):11-21.

121. Dorschner MO, Amendola LM, Turner EH, et al. Actionable, pathogenic incidental findings in 1,000 participants' exomes. Am J Hum Genet 2013;93(4):631-40.

122. Rogozin IB, Pavlov YI. Theoretical analysis of mutation hotspots and their DNA sequence context specificity. Mutation Research/Reviews in Mutation Research 2003;544(1):65-85.

123. Nagy E, Maquat LE. A rule for termination-codon position within intron-containing genes: When nonsense affects RNA abundance. Trends Biochem Sci 1998;23(6):198-9.

124. van den Hurk JA, Hendriks W, van de Pol DJ, et al. Mouse choroideremia gene mutation causes photoreceptor cell degeneration and is not transmitted through the female germline. Hum Mol Genet 1997;6(6):851-8.

125. Alory C, Balch WE. Organization of the rab-GDI/CHM superfamily: The functional basis for choroideremia disease. Traffic 2001;2(8):532-43.

126. Bentley DR, Balasubramanian S, Swerdlow HP, et al. Accurate whole human genome sequencing using reversible terminator chemistry. Nature 2008;456(7218):53-9.

127. Genead MA, Fishman GA. Cystic macular oedema on spectral-domain optical coherence tomography in choroideremia patients without cystic changes on fundus examination. Eye (Lond) 2011;25(1):84-90.

128. Kedar S, Ghate D, Corbett JJ. Visual fields in neuro-ophthalmology. Indian J Ophthalmol 2011;59(2):103-9.

129. Bittner AK, Iftikhar MH, Dagnelie G. Test-retest, within-visit variability of goldmann visual fields in retinitis pigmentosa. Invest Ophthalmol Vis Sci 2011;52(11):8042-6.

130. Esterman B. Grid for scoring visual fields. II. perimeter. Arch Ophthalmol 1968;79(4):400-6.

131. Zahid S, Peeler C, Khan N, et al. Digital quantification of goldmann visual fields (GVFs) as a means for genotype-phenotype comparisons and detection of progression in retinal degenerations. Adv Exp Med Biol 2014;801131-7.

132. Langelaan M, Wouters B, Moll AC, et al. Functional field score: The effect of using a goldmann V-4e isopter instead of a goldmann III-4e isopter. Invest Ophthalmol Vis Sci 2006;47(5):1817-23.

133. Sample PA, Dannheim F, Artes PH, et al. Imaging and perimetry society standards and guidelines. Optom Vis Sci 2011;88(1):4-7.

134. Webster A. Longitudinal imaging data from a cohort of choroideremia patients in the UK ; how to monitor treatment efficacy? In: 1er International Choroideremia Research Symposium; Sommieres, France: 2011.

135. Wu Z, Ayton LN, Guymer RH, et al. Low-luminance visual acuity and microperimetry in age-related macular degeneration. Ophthalmology 2014;(Epub ahead of print).

136. Field GD, Sampath AP, Rieke F. Retinal processing near absolute threshold: From behavior to mechanism. Annu Rev Physiol 2005;67491-514.

137. Kiser AK, Mladenovich D, Eshraghi F, et al. Reliability and consistency of dark-adapted psychophysical measures in advanced eye disease. Investigative Ophthalmology & Visual Science 2006;47(1):444-52.

138. Glickman RD. Ultraviolet phototoxicity to the retina. Eye Contact Lens 2011;37(4):196-205.

139. Duncan JL, Aleman TS, Gardner LM, et al. Macular pigment and lutein supplementation in choroideremia. Exp Eye Res 2002;74(3):371-81.

140. Abstracts of the 50th ISCEV (international society for clinical electrophysiology of vision) international symposium. june 3-7, 2012. valencia, spain. Doc Ophthalmol 2012;124 Suppl 11-68.

141. Zhou Q, Weis E, Ye M, et al. An internet-based health survey on the co-morbidities of choroideremia patients. Ophthalmic Physiol Opt 2013;33(2):157-63.

142. Lowenstein PR. Clinical trials in gene therapy: Ethics of informed consent and the future of experimental medicine. Curr Opin Mol Ther 2008;10(5):428-30.

Tables

Table 3-1 *CHM* Mutations

Family	Mutation	Exon	Protein Change	Previous Reports
1	c.-29-?_*3450+?del	1-15	Complete gene deletion - REP-1 absent	Cremers *et al.*, 1990
2	c.-29-?_*3450+?del	1-15	Complete gene deletion - REP-1 absent	
3	c.-29-?_*3450+?del	1-15	Complete gene deletion - REP-1 absent	
4	c.-29-?_*3450+?del	1-15	Complete gene deletion - REP-1 absent	
5	c.-29-?_*3450+?del	1-15	Complete gene deletion - REP-1 absent	
6	c.-29-?_*3450+?del	1-15	Complete gene deletion - REP-1 absent	
7	c.-29-?_*3450+?del	1-15	Complete gene deletion - REP-1 absent	
8	c.-29-?_*3450+?del	1-15	Complete gene deletion - REP-1 absent	
9	c.-29-?_*3450+?del	1-15	Complete gene deletion - REP-1 absent	
10	c.-29-(57-63kb)_49+?del	1	Deletion of exon 1 – REP-1 absent	First reported by van den Hurk *et al.*, 1997
11	c.-29-(57-63kb)_49+?del	1	Deletion of exon 1 – REP-1 absent	REP-1 absence confirmed by McTaggart *et al.*, 2002
12	c.-29-(57-63kb)_49+?del	1	Deletion of exon 1 – REP-1 absent	
13	c.-29-?_49+?del	1	Deletion of exon 1 – REP-1 absent	
14	c.3G>A	1	Affects start codon – REP-1 absent	Strunnikova *et al.*, 2009
15	c.25_28delTTTG insAGTAATAGTAA	1	p.Phe9Serfs*14	
16	c.37delG	1	p.Val13*	
17	c.49+1G>A	intron 1	Splice site mutation	
18	c.49+3A>G	intron 1	Splice site mutation	
19	c.49+3A>G	intron 1	Splice site mutation	
20	c.49+3A>G	intron 1	Splice site mutation	
21	c.50-?_314+?del	2-4	Deletion of exons 2-4 - (out-of-frame)	
22	c.116+1G>T	intron 2	p.Gly17Glufs*21	Esposito *et al.*, 2011
23	c.116+1G>C	intron 2	Splice site mutation	
24	c.116+1G>C	intron 2	Splice site mutation	
25	c.116+1G>C	intron 2	Splice site mutation	
26	c.117-?_1166+?dup	3-8	Duplication of exons 3-8 – unable to predict	Chi *et al.*, 2012
27	c.117-?_1510+?dup	3-12	Duplication of exons 3-12 –	

Table 3-1 – Continued

Family	Mutation	Exon	Protein Change	Previous Reports
			unable to predict	
28	c.167dupT	3	p.Leu56Phefs*12	
29	c.190-2A>G	intron 3	Splice site mutation – p.Glu64*	van den Hurk *et al.*, 2003
30	c.225G>A	4	p.Trp75*	
31	c.232C>T	4	p.Gln78*	
32	c.315-?_1166+?del	5-8	Deletion of exons 5-8 - (in-frame) – REP-1 absent	McTaggart *et al.*, 2002
33	c.316C>T	5	p.Gln106*	Nesslinger *et al.,* 1996
34	c.470_473delAAAC	5	p.Gln157Leufs*10	
35	c.525_526delAG	5	p.Glu177Lysfs*6	van Bokhoven *et al.*, 1994
36	c.525_526delAG	5	p.Glu177Lysfs*6	
37	c.525_526delAG	5	p.Glu177Lysfs*6	
38	c.563_564delTG	5	p.Val188Alafs*10	McDonald *et al.*, 2004
39	c.564_565delGC	5	p.Pro189Ilefs*11	Fujiki *et al.*, 1999
40	c.652_655delTCAC	5	p.Ser218Lysfs*13	McTaggart *et al.*, 2002
41	c.653C>G	5	p.Ser218*	
42	c.700A>T	5	p.Lys234*	Strunnikova *et al.*, 2009
43	c.700A>T	5	p.Lys234*	
44	c.703-?_940+?del	6-7	Deletion of exons 6-7 - p.Leu235Argfs*4	Strunnikova *et al.*, 2009
45	c.703-?_940+?del	6-7	Deletion of exons 6-7 - p.Leu235Argfs*4	Truncated product confirmed by Esposito *et al.*, 2011
46	c.703-?_940+?del	6-7	Deletion of exons 6-7 - p.Leu235Argfs*4	
47	c.703-?_1166+?del	6-8	Deletion of exons 6-8 - (out-of-frame)	
48	c.715C>T	6	p.Arg239*	McTaggart *et al.*, 2002
49	c.715C>T	6	p.Arg239*	
50	c.757C>T	6	p.Arg253*	Fujiki *et al.*, 1999
51	c.757C>T	6	p.Arg253*	
52	c.757C>T	6	p.Arg253*	
53	c.757C>T	6	p.Arg253*	
54	c.757C>T	6	p.Arg253*	
55	c.757C>T	6	p.Arg253*	
56	c.757C>T	6	p.Arg253*	
57	c.757C>T	6	p.Arg253*	
58	c.757C>T	6	p.Arg253*	
59	c.757C>T	6	p.Arg253*	
60	c.799C>T	6	p.Arg267*	van den Hurk *et al.*, 1997
61	c.799C>T	6	p.Arg267*	
62	c.799C>T	6	p.Arg267*	
63	c.799C>T	6	p.Arg267*	
64	c.799C>T	6	p.Arg267*	
65	c.808C>T	6	p.Arg270*	Fujiki *et al.*, 1999
66	c.808C>T	6	p.Arg270*	
67	c.808C>T	6	p.Arg270*	

Table 3-1 – Continued

Family	Mutation	Exon	Protein Change	Previous Reports
68	c.817C>T	6	p.Gln273*	Strunnikova *et al.*, 2009
69	c.819G>T	6	p.Gln273His	
70	c.820-1G>C	intron 6	Splice site mutation – skips exon 7, absent REP-1	Potter *et al.*, 2004
71	c.846delT; c.881G>T	7	p.Phe282Leufs*9 (c.881 is beyond the premature stop codon)	
72	c.877C>T	7	p.Arg293*	Van Bokhoven *et al.*, 1994
73	c.877C>T	7	p.Arg293*	
74	c.885_886insA	7	p.Met296Asnfs*11	
75	c.889A>T	7	p.Lys297*	
76	c.894delT	7	p.Thr300Hisfs*25	
77	c.910G>T	7	p.Glu304*	
78	c.993delC	8	p.Asn332Thrfs*12	
79	c.1034C>G	8	p.Ser345*	Fujiki *et al.*, 1999
80	c.1167-?_1413+?del	9-11	Deletion of exons 9-11 - (out-of-frame)	
81	c.1184delG	9	p.Gly395Valfs*14	
82	c.1194T>G	9	p.Tyr398*	Huang *et al.*, 2012
83	c.1218C>A	9	p.Cys406*	Nesslinger *et al.*, 1996
84	c.1218C>A	9	p.Cys406*	
85	c.1234G>T	9	p.Glu412*	
86	c.1273C>T	10	p.Gln425*	
87	c.1327_1328delAT	10	p.Met443Valfs*18	Strunnikova *et al.*, 2009
88	c.1350-6T>G	intron 10	Skip exon 11 - p.Arg450Argfs*4[b]	McTaggart *et al.*, 2002
89	c.1350-2A>C	intron 10	Splice site mutation	Renner *et al.*, 2009
90	c.1350-(14-10)delTTGT	intron 10	Small deletion affecting a splice site	
91	c.1363delG	11	p.Ala455Glnfs*3	Nesslinger *et al.*, 1996
92	c.1370T>C	11	p.Leu457Pro	
93	c.1511-?_1609+?del	13	Deletion of exon 13 - (in-frame)	
94	c.1511-1G>A	intron 12	Splice site mutation	
95	c.1511-1G>A	intron 12	Splice site mutation	
96	c.1512T>A	13	p.Tyr504*	McTaggart *et al.*, 2002
97	c.1584_1587delTGTT	13	p.Val529Hisfs*7	van den Hurk *et al.*, 1992
98	c.1603G>T	13	p.Glu535*	McTaggart *et al.*, 2002
99	c.1624G>T	14	p.Glu542*	
100	c.1624delG	14	p.Glu542Leufs*13	Jacobson *et al.*, 2006
101	c.1649T>C	14	p.Leu550Pro	Sergeev *et al.*, 2009
102	C.1670C>A	14	p.Ser557*	
103	C.1670C>A	14	p.Ser557*	
104	c.1670C>A	14	p.Ser557*	
105	c.1697_1698delAT	14	p.Asn566Argfs*19	
106	c.238C>T; c.1327A>G	4, 10	p.Leu80Phe; p.Met443Val	c.238C>T dbSNP #rs55741408

Table 3-2 Demographic and Clinical Features of Subjects

	Age Group	1-10	11-20	21-30	31-40	41-50	51-60	61-70	71-80
Visual Acuity[a]	n	10	28	17	19	24	15	12	3
	Age (mean ±SD)	8.3 ±1.2	16.0 ±2.7	25.5 ±2.8	36.0 ±2.9	46.0 ±2.7	54.6 ±2.3	65.2 ±3.1	72.7 ±1.2
	Age (median)	9	17	26	37	46	55	64	72
	VA (mean ±SD)	0.075 ±0.118	0.045 ±0.126	0.016 ±0.059	0.099 ±0.172	0.372 ±0.497	0.818 ±0.765	0.848 ±0.845	2.567 ±0.231
	VA (median)	0.05	0	0	0	0.3	0.5	0.439	2.7

	Age Group	1-10	11-20	21-30	31-40	41-50	51-60	61-70	71-80
Visual Field[b]	n	5	16	7	7	15	10	4	0
	Age (mean ±SD)	8.8 ±0.5	15.6 ±2.6	25.9 ±2.5	35.3 ±3.1	45.9 ±2.6	54.3 ±2.9	65.0 ±2.8	
	Age (median)	9	15.5	26	37	46	54.5	64	
	VF (mean ±SD)	73±51	74±56	42±45	19±11	13±9	6±6	4±2	
	VF (median)	60	50	25	15	12	5	4	

[a] Visual acuities are in logMAR units. The VA of the better eye is used.

[b] Visual fields are defined as the width of the continuous visual field across the horizontal meridian (in degrees) using a Goldmann perimeter with the III4e isopter. The VF of the better eye is used.

Table 3-3 Visual Acuity of Subjects Grouped by Severity

Age Group (years)	1-10	11-20	21-30	31-40	41-50	51-60	61-70	71-80	Total
≤20/40 (≤0.3 logMAR)	10/10 (100%)	27/28 (96%)	17/17 (100%)	18/19 (95%)	13/24 (54%)	5/15 (33%)	3/12 (25%)	0/3	93/128 (73%)
>20/40 to ≤20/70 (>0.3 to ≤0.54 logMAR)	0/10	1/28 (4%)	0/17	1/19 (5%)	8/24 (33%)	3/15 (20%)	4/12 (33%)	0/3	17/128 (13%)
>20/70 to ≤20/200 (>0.54 to ≤1.0 logMAR)	0/10	0/28	0/17	0/19	2/24 (8%)	3/15 (20%)	2/12 (17%)	0/3	7/128 (5%)
>20/200 (>1.0 logMAR)	0/10	0/28	0/17	0/19	1/24 (4%)	4/15 (27%)	3/12 (25%)	3/3 (100%)	11/128 (9%)

Figures

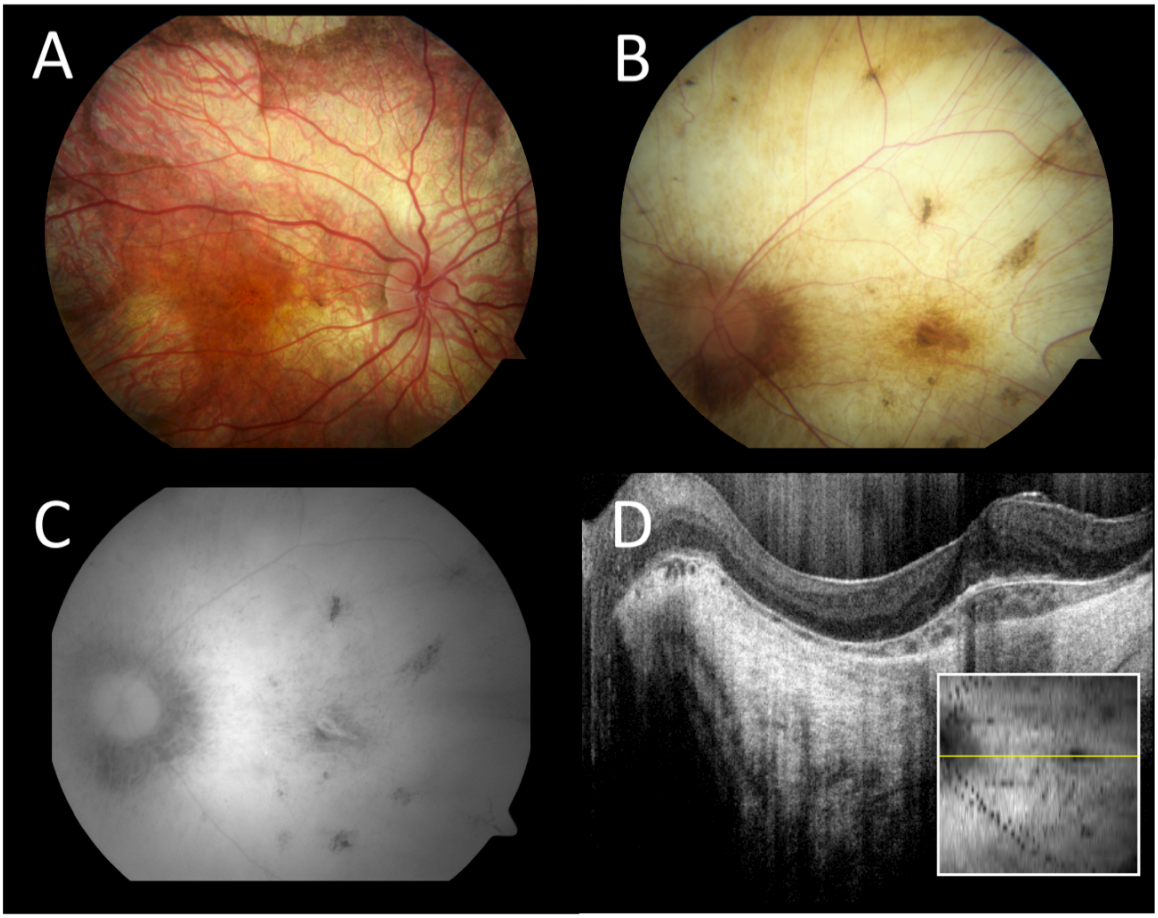

Figure 1-1. Fundus photographs of a 15 year old male (A) and a 51 year old male (B) with choroideremia. The younger male has patchy RPE degeneration exposing the underlying choroidal vasculature; in panel B, the peripheral choroid is completely eliminated and only bare sclera is visible. A corresponding fundus autofluorescence image (C) from the 51 year old male shows an island of relative hyperfluorescence from the surviving RPE tissue. An OCT slice (D; inset shows the retina location) demonstrates complete degeneration of the retina, RPE, and choroid outside of the remaining retinal island.

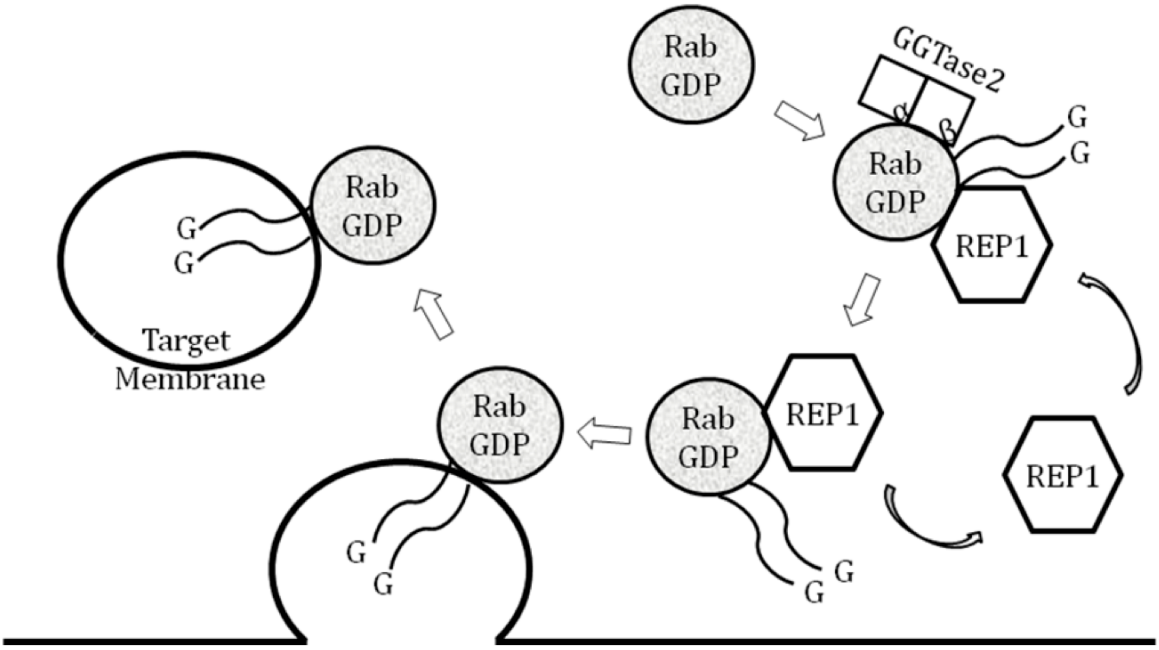

Figure 1-2. Schematic diagram demonstrating the interaction of REP-1, Rab GGTase-2, Rab proteins, and GGPP. REP-1 and the GGTase-2 heterodimer form an initial complex that associates with Rab proteins and catalyzes Rab prenylation with GGPP. The complex dissociates and REP-1 escorts the prenylated Rab-GG to its target membrane, where REP-1 recycles to form a new REP-1:GGTase-2 complex. (Adapted from Freund & MacDonald, 2012)

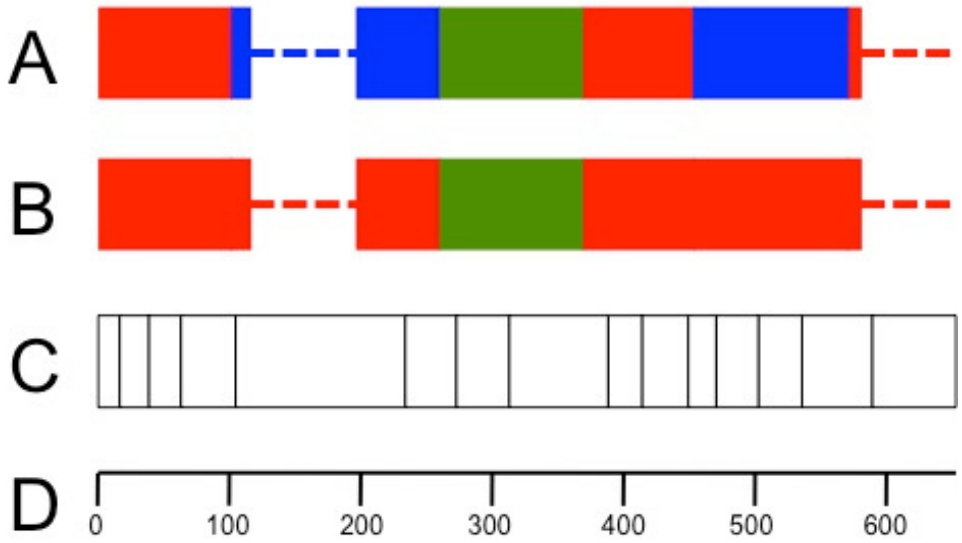

Figure 1-3. Structural domains of REP-1 protein proposed by Sergeev *et al.* [57] and by Alory and Balch [125]. Sergeev *et al.* developed a 3-domain model (A) where domains 1 & 2 (red and blue) form the Rab binding platform (RBP) and domain 3 (green) associates with GGTase-2. The portions of the protein not visualized in crystal structures are drawn with a dotted line. Alory and Balch describe a 2-domain model (B): domain 1 (red) interacts with Rab proteins via the RBP and domain 2 (green) interacts with GGTase-2. The relative sizes of the exons (C) and the protein sequence (D) are shown.

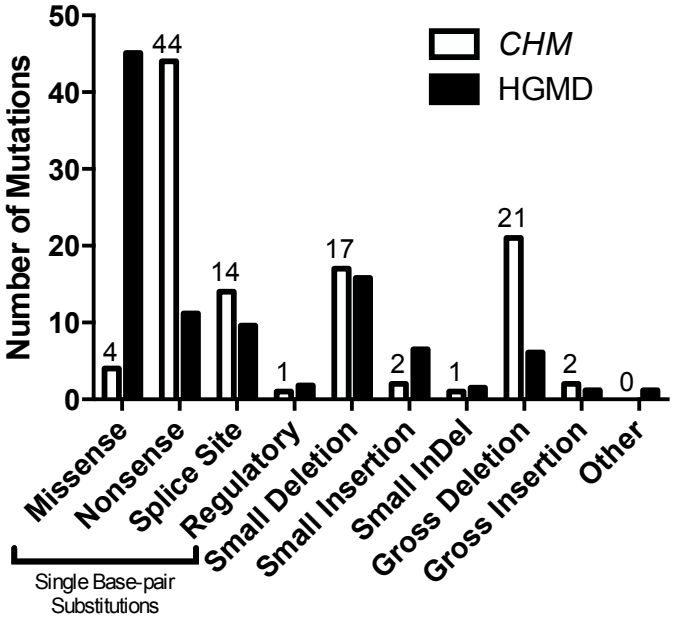

Figure 3-1. Proportion of *CHM* mutations observed in 106 affected families compared to the mutations reported in the Human Genome Mutation Database (HGMD). Only 4% of *CHM* mutations are missense substitutions, compared to 45% of mutations in the HGMD. All of the detected deletions cause a shift in the reading frame and premature truncation of the REP-1 protein.

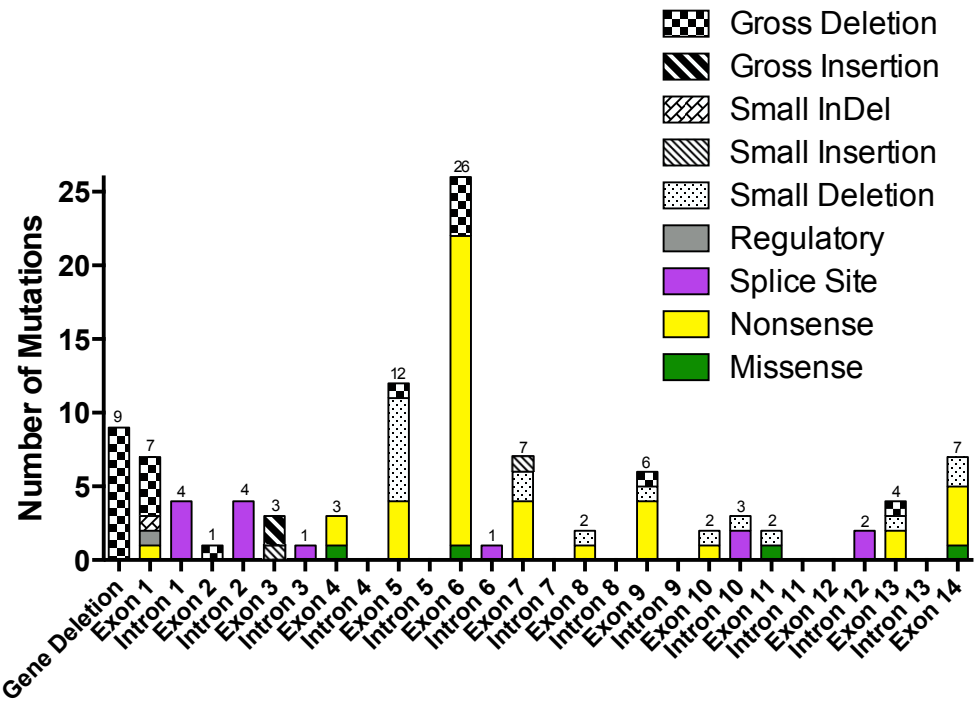

Figure 3-2. The exon and intron locations of mutations in the *CHM* gene observed in 106 affected families. The frequency and location of each mutation type is demonstrated. A cluster of nonsense mutations occurs on exon 6.

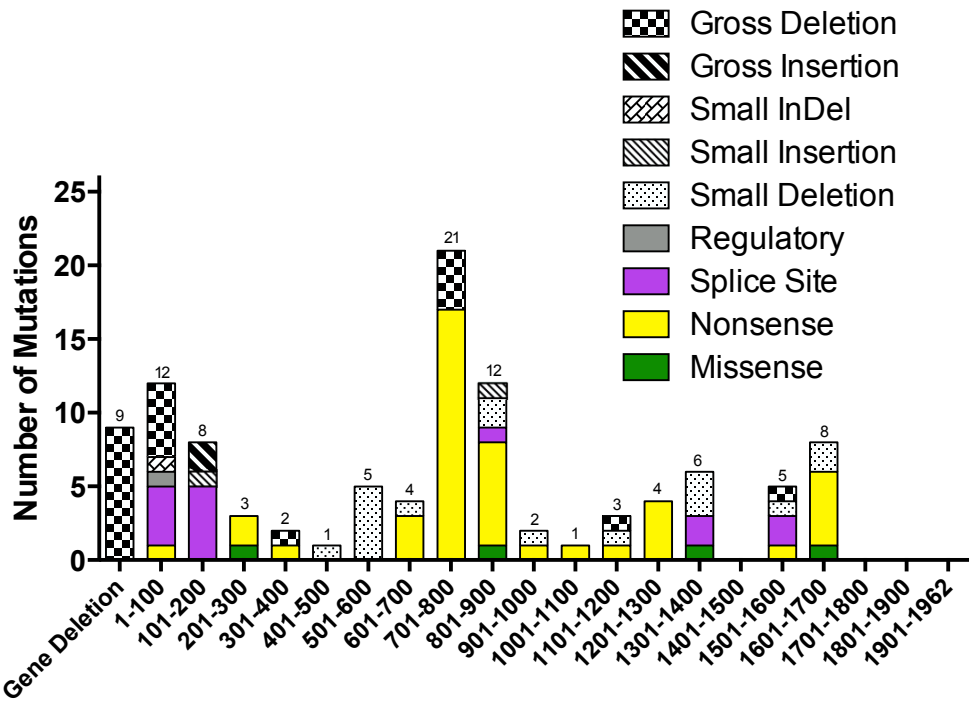

Figure 3-3. The location of mutations along the *CHM* cDNA sequence. Intron mutations are depicted as occurring at the next 3' exon nucleotide downstream. A cluster of nonsense mutations that occur from c.701-800 corresponds to exon 6 (which spans nucleotides c.703-819).

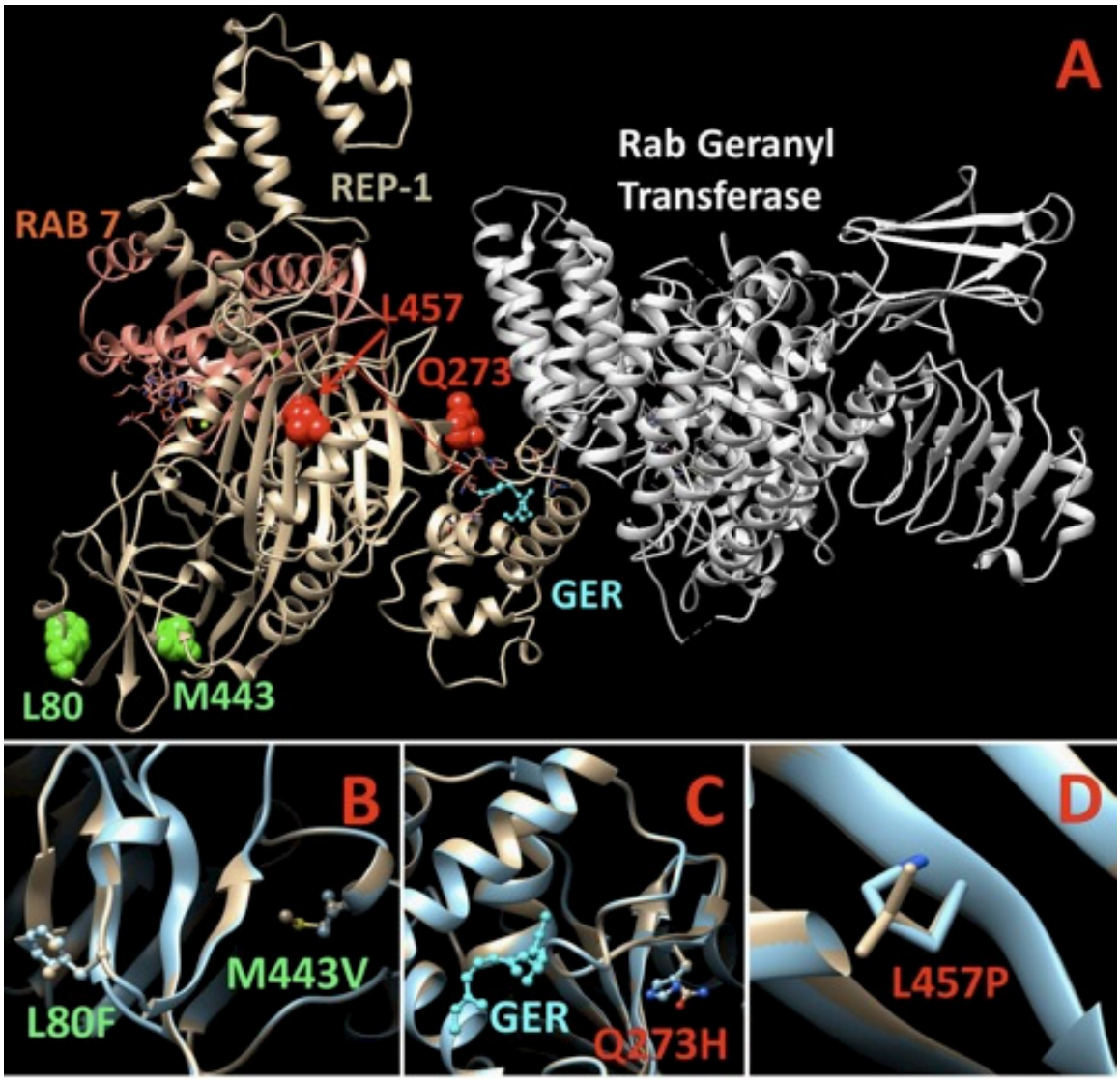

Figure 3-4. The structure of REP-1 (beige) in relation to Rab Geranyl Transferase (white) and Rab7 (pink) and its substrate geranylgeranyl (GER; blue). The *CHM* double mutant, L80F and M443V, is highlighted in panel B (green); the Q273H (red) and L457P (red) mutations are in panels C and D, respectively. (Modelling provided by Yuri Sergeev, National Eye Institute, Bethesda, MD)

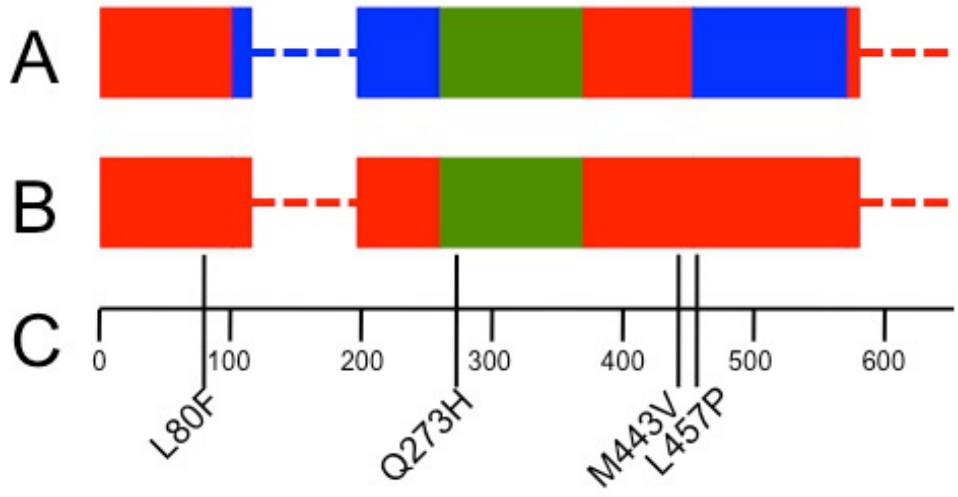

Figure 3-5 The locations of four novel *CHM* missense mutations with respect to the REP-1 protein domains proposed Sergeev *et al.* (A) [57] and by Alory and Balch (B) [125]. The missense mutations are shown along the primary structure of REP-1 (C): 3 of the missense mutations are located within domain 1, which is responsible for the association of REP-1 with Rab proteins. The p.Q273H substitution is located on the β-sheet linking domains 1 and 2.

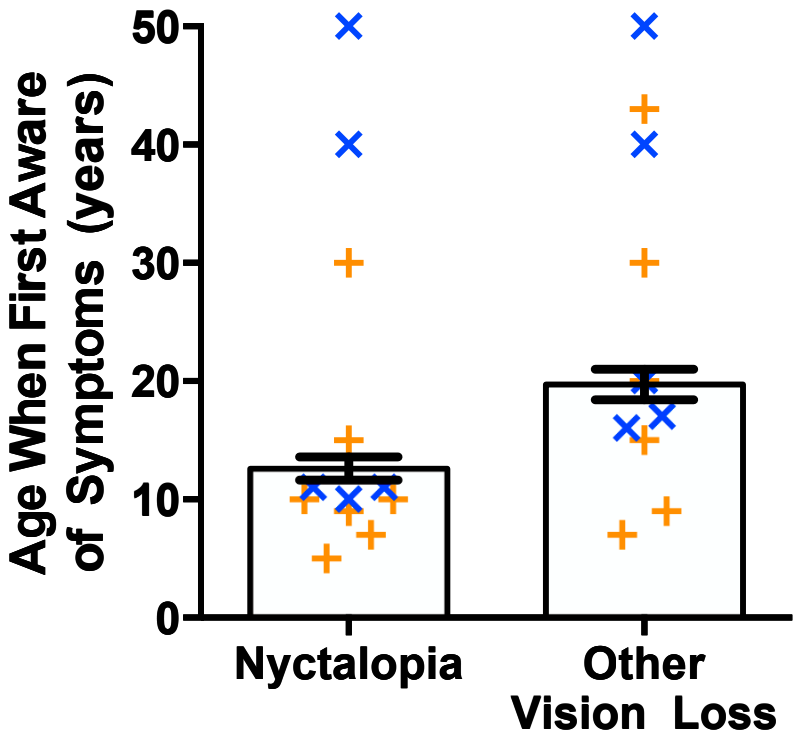

Figure 3-6. The self-reported age of onset (in years) of symptoms by males affected by choroideremia. The age of onset of nyctalopia is 12.6±1.0 years (mean±SEM, n=71). The age of onset of other symptoms of vision loss is 19.7±1.3years (mean±SEM , n=72). The onset of symptoms in individuals with missense mutations is indicated by an orange +; the onset of symptoms in individuals who do not express any REP-1 due to whole gene deletions or deletions of the ATG start codon is indicated by a blue ×.

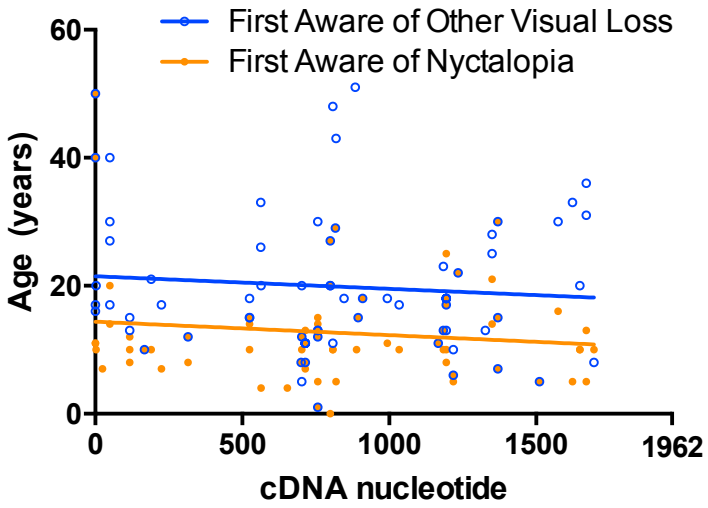

Figure 3-7. The onset of subjective symptoms compared to the *CHM* cDNA location of individuals' mutations. There is no pattern suggesting that the length of functional cDNA affects the age of onset of symptoms. Linear regression analyses demonstrate that the age of onset of nyctalopia and the age of onset of visual symptoms are not significantly associated with the length of functional cDNA (p=0.29 and p=0.47 respectively).

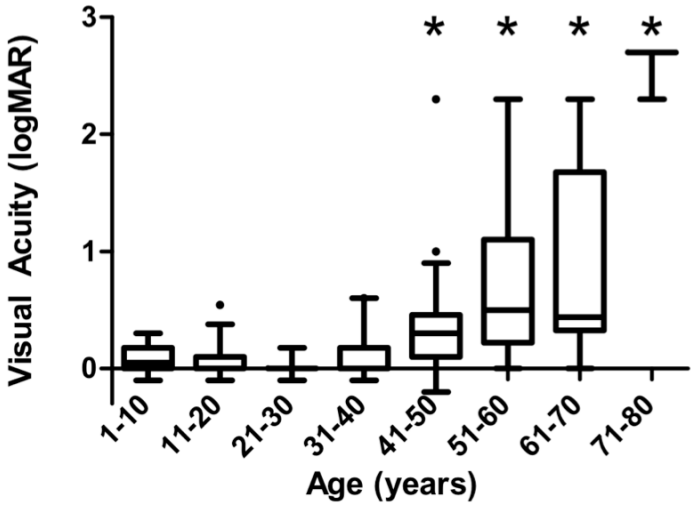

Figure 3-8. The median visual acuity (logMAR equivalent) of males grouped by decade (n=128). The whiskers are plotted with the Tukey method and outliers are noted. Groups which differ significantly ($p<0.05$) from baseline, according to the inclusion-exclusion test method, are indicated by *. The critical age for visual acuity is 40 years of age, above which males are at increased risk of declining visual acuity.

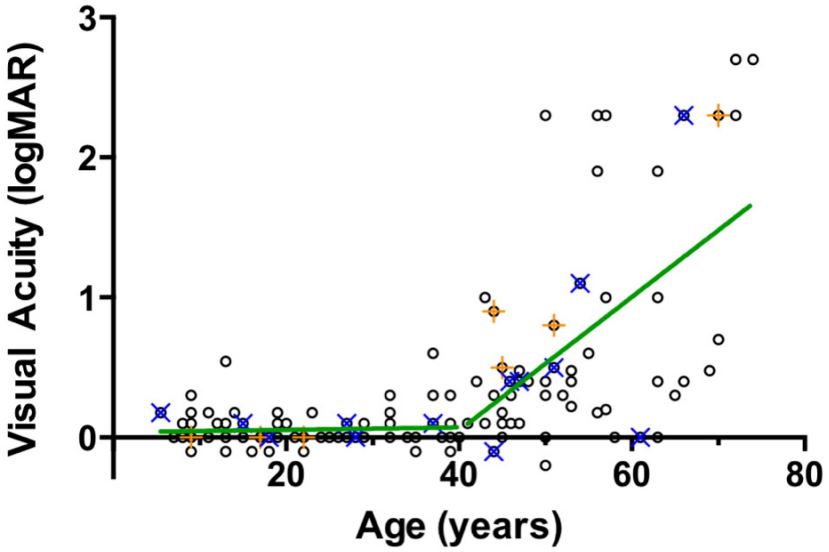

Figure 3-9. The visual acuity (logMAR equivalent) of affected males' better eye as a function of age (n=128). The sample population is divided at the critical age (40 years old) into the ≤40 years old group or the >40 years old group. Individuals with missense mutations are indicated by an orange +; individuals who do not express any REP-1 due to whole gene deletions or deletions of the ATG start codon are indicated by a blue ×. The rate of change of visual acuity predicted by a linear regression model (green line) in the ≤40 years old group is not significantly different from 0 (p=0.71); the rate of change of visual acuity in the >40 years old group is 0.0483 logMAR units/year (p=0.001).

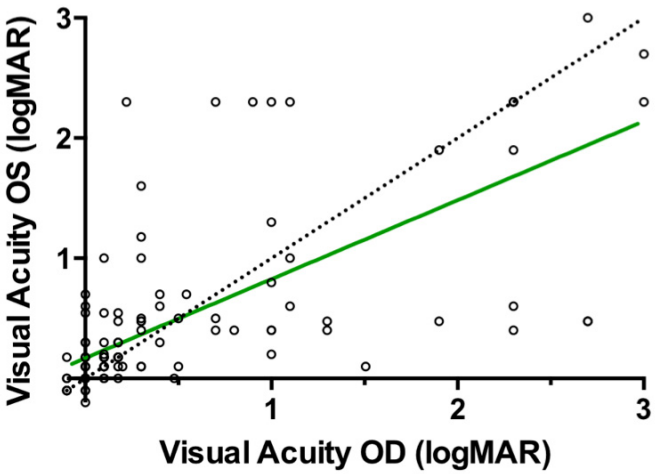

Figure 3-10. The inter-eye correlation of the visual acuities (logMAR) of affected males. A perfect correlation is also plotted for comparison (dotted line). The visual acuities of individuals' eyes are highly correlated (Spearman r=0.76).

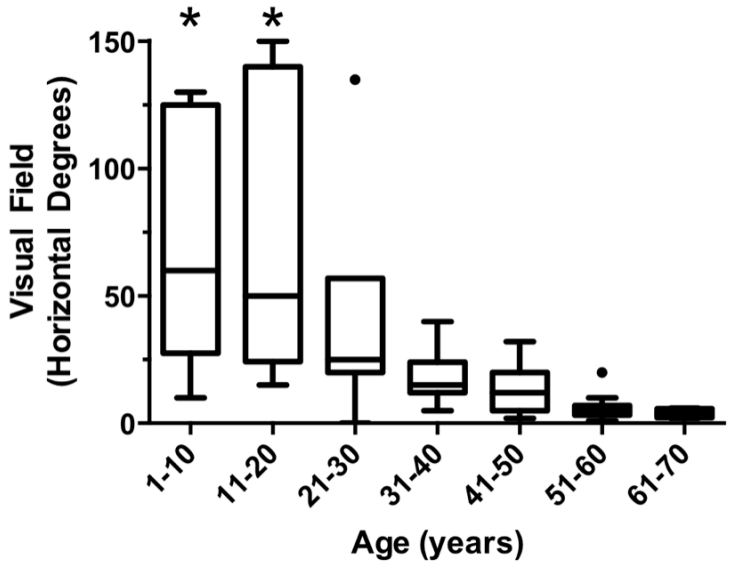

Figure 3-11. The median visual field (the continuous visual field across the horizontal meridian, in degrees) of males grouped by decade (n=64). The whiskers are plotted with the Tukey method and outliers are noted. Groups which differ significantly ($p<0.05$), according to the inclusion-exclusion test method, are indicated by *. The critical age for visual field changes is 20 years old: prior to this age, visual field assessments are highly variable and difficult to predict progression.

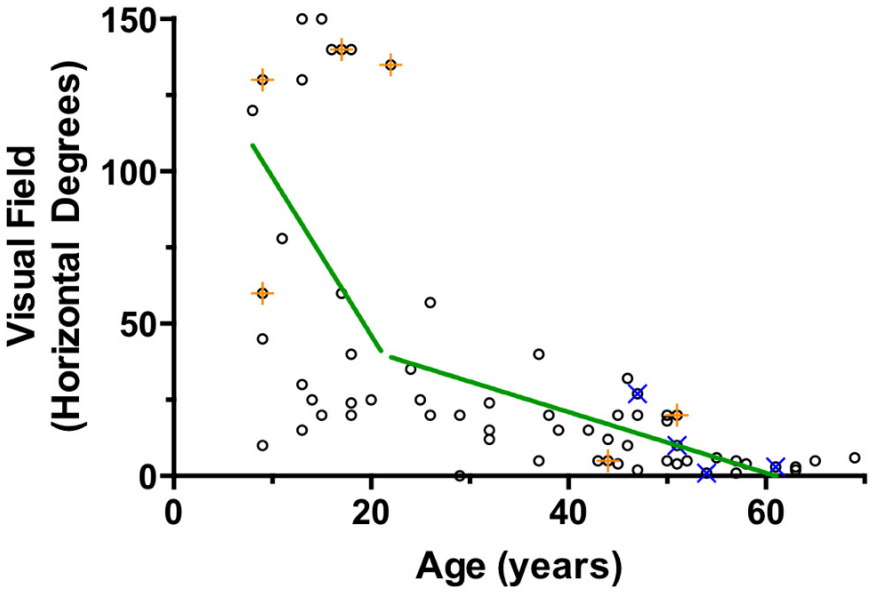

Figure 3-12. The visual field (the continuous visual field across the horizontal meridian, in degrees) of affected males' better eye as a function of age (n=64). The sample population was divided at the critical age (20 years old), separating individuals into the ≤20 years old group and the >20 years old group. Individuals with missense mutations are indicated by an orange +; individuals who do not express any REP-1 due to whole gene deletions or deletions of the ATG start codon are indicated by a blue ×. In a linear regression model (green line), age was not a significant predictor of visual field in the ≤20 years old group (p=0.785); the rate of change of visual fields in the >20 years old group is a loss of 0.868 horizontal degrees per year (p=0.005).

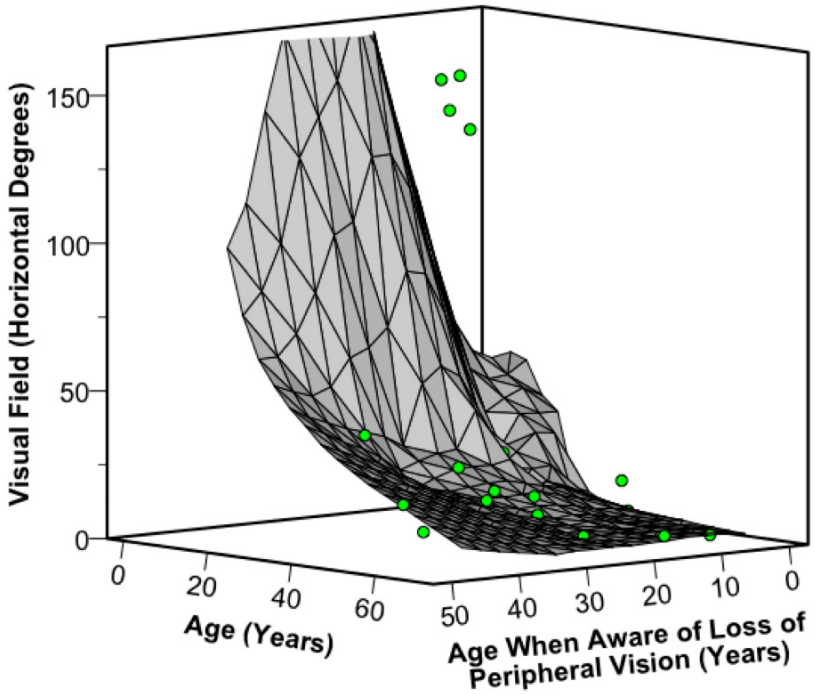

Figure 3-13. The visual field (the continuous visual field across the horizontal meridian, in degrees) of affected males' better eye as a function of age and age of onset of visual symptoms (other than nyctalopia). Both factors predicted visual field loss in individuals older than 20 years of age (p=0.00005). The visual fields decrease by 1.224 horizontal degrees per year of age. Later onset of symptoms predicts larger visual fields: every symptom-free year corresponds to 1.228 more horizontal degrees of visual field.

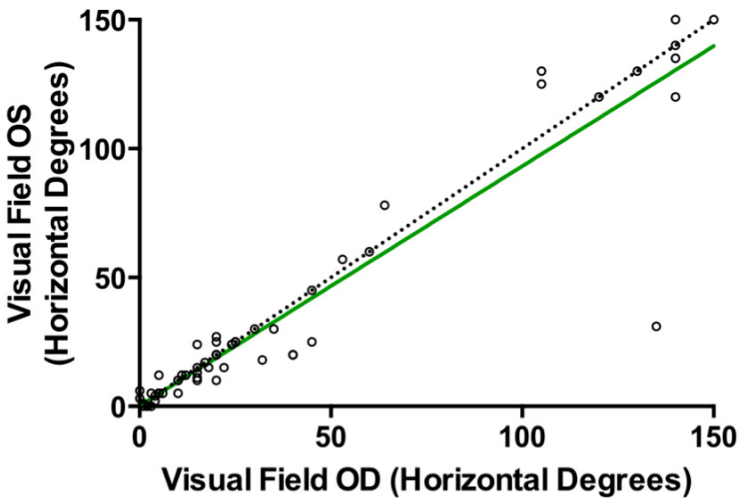

Figure 3-14. The inter-eye correlation of the visual fields (horizontal degrees across the meridian) of affected males. A perfect correlation is plotted for comparison (dotted line). The visual fields of individuals' eyes are very highly correlated (Spearman r=0.95).

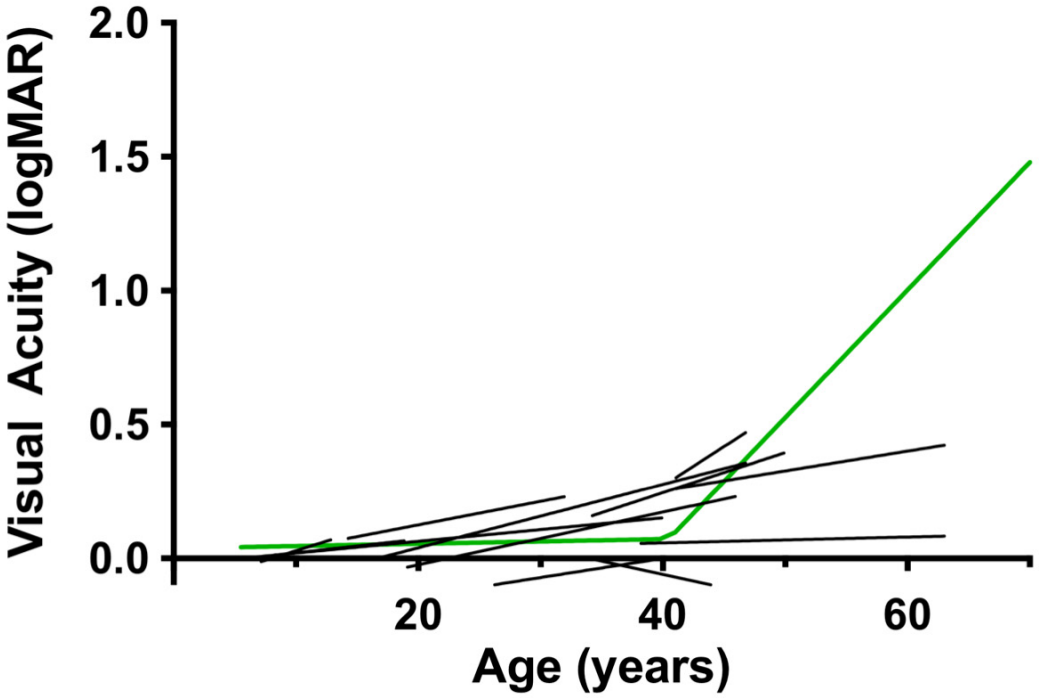

Figure 3-15. Longitudinal analysis of the visual acuities (logMAR equivalent) of 12 affected males. Black lines represent the linear regressions fit to each individual's disease progression and are plotted with the predicted natural history based on the cross-sectional study (green line). No precipitous decline in visual acuity was observed in any of the individuals, even in those above the age of 40 years old.

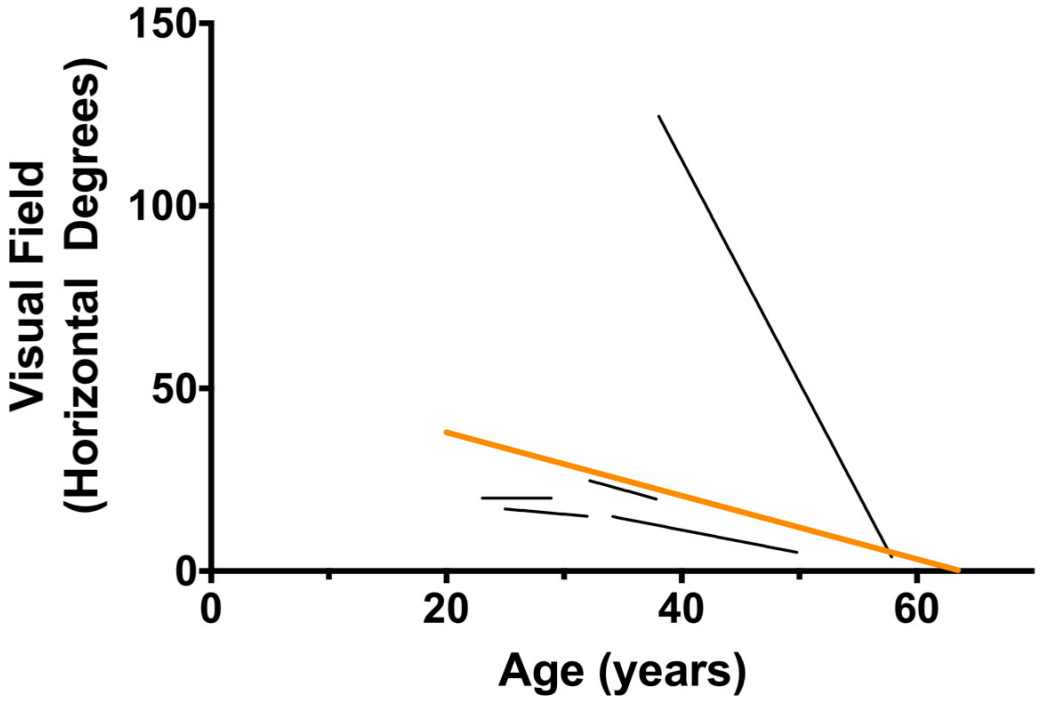

Figure 3-16. Longitudinal analysis of the visual fields (horizontal degrees across the meridian) of 5 affected males. Black lines represent the linear regressions fit to each individual's disease progression and are plotted with the predicted natural history based on the cross-sectional study (green line). 80% of the individuals progressed at the predicted rate of visual field loss.

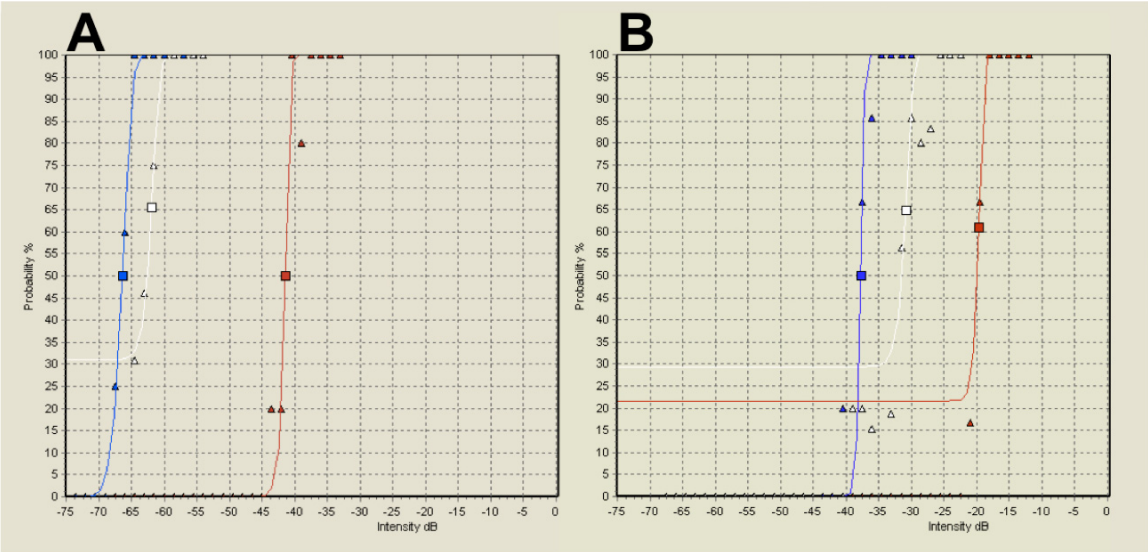

Figure 3-17. Representative full-field stimulus threshold responses in an unaffected 58 year old (A) and a 40 year old male with choroideremia (B). The threshold sensitivities to blue, white, and red stimuli are tested and the percent of 'yes' responses at each stimulus intensity are plotted (blue, white, and red Δ, respectively). The Weibull statistical curve calculates the threshold intensity. False positive and false negative responses cause the statistical function to modify the threshold (*e.g.*, the raised floor of the curve for the white stimuli in both examples).

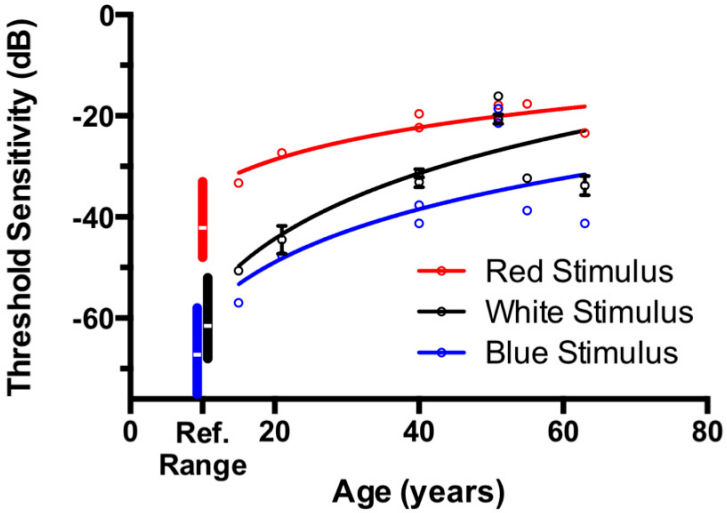

Figure 3-18. The full-field thresholds of eight males affected by choroideremia, tested monocularly. White stimuli were tested in triplicate (black circle, mean±SD), and the blue and red stimuli were each tested once (blue and red circles, respectively). Reference ranges and means in a normal sample are shown (coloured bars and white line, respectively). The rod-dominated sensitivity to blue and white stimuli decreases at a faster rate compared to the cone-dominant threshold sensitivity to red stimuli.

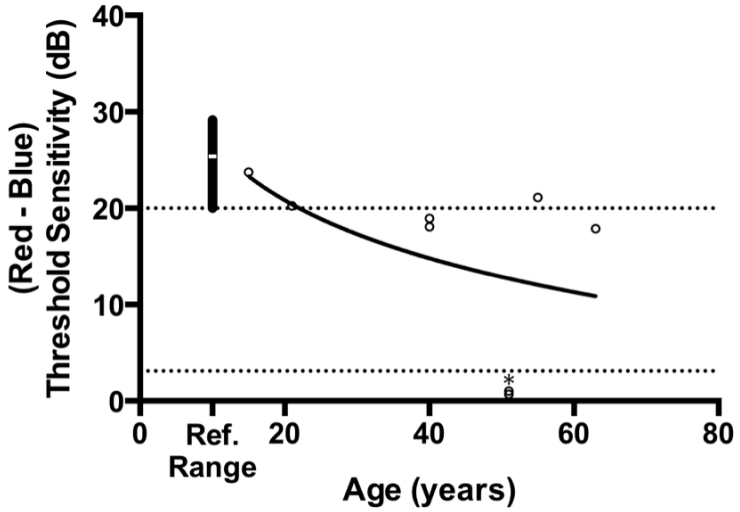

Figure 3-19. Differences in threshold sensitivities to blue and red stimuli of eight affected males (circles). The reference range and mean from a normal sample (black bar and white line respectively) represents a rod-dominant threshold response. Sensitivity differences <20 dB but >3.1 dB (dotted lines) indicate a mixed rod & cone contribution to perception. The two individuals (*) with sensitivity differences <3.1 dB have purely cone-mediated perception.

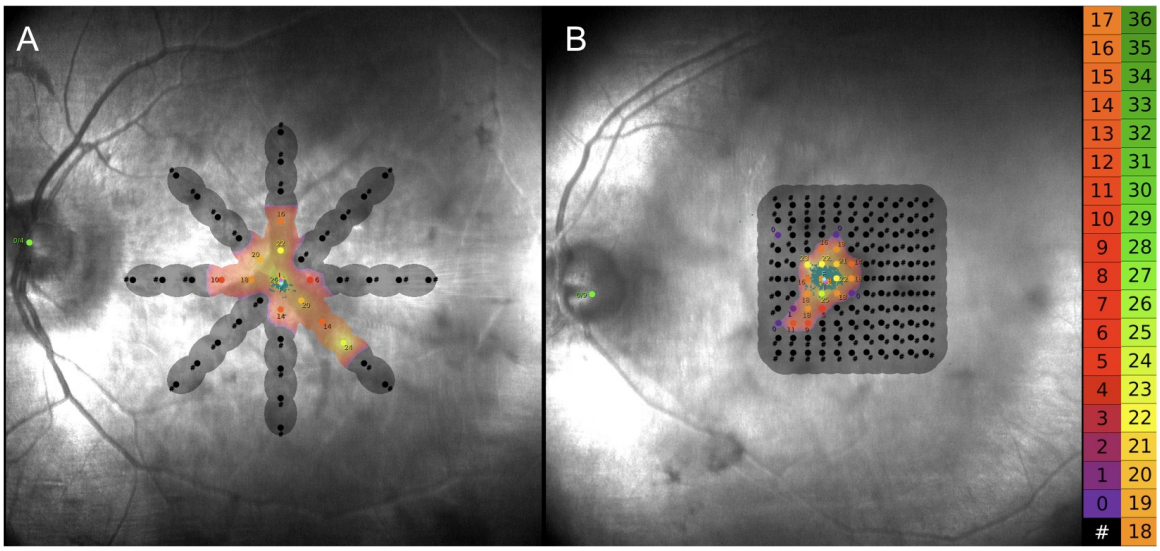

Figure 3-20. Representative microperimetry sensitivity maps of a 40 year old male (A) and a 63 year-old male (B) with choroideremia. These maps were generated by the Centervue MAIA microperimeter with a 20° grid in a spoke pattern (A) and a custom 11×11 grid (B) using a 4-2 step testing strategy. The maximum (brightest) stimulus intensity (0 dB) is 318 cd/m^2; if the 0 dB stimulus is not detected, it is denoted by a # symbol.